Cell

Control of mammalian locomotion by ventral spinocerebellar tract neurons

Graphical abstract

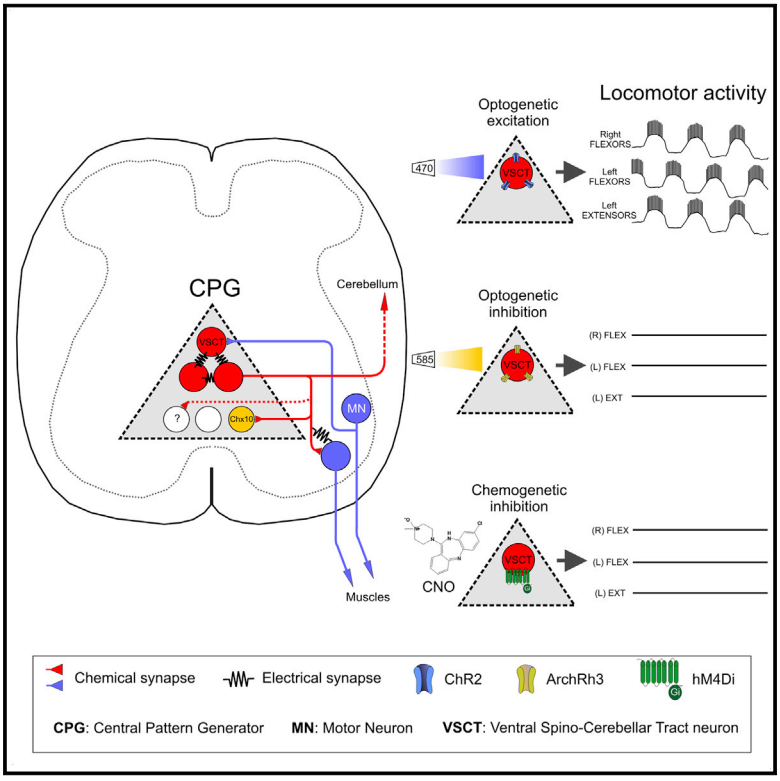

Highlights

- VSCTs have rhythmogenic properties, form circuits with motor neurons and Chx10^{+} neurons
- VSCTs can be activated monosynaptically and electrically by motor neurons
- Activation of VSCTs is sufficient to initiate locomotion during early development
- Silencing VSCTs abolishes locomotor behavior in neonates and perturbs it in adulthood

Authors

Joshua I. Chalif, María de Lourdes Martínez-Silva, John G. Pagiazitis, Andrew J. Murray, George Z. Mentis

Correspondence

gzmentis@columbia.edu

In brief

Ventral spinocerebellar tract neurons (VSCTs) are necessary and sufficient to drive generation and maintenance of locomotor behavior in mice.

Chalif et al., 2022, Cell *185*, 328–344
January 20, 2022
https://doi.org/10.1016/j.cell.2021.12.014

CellPress

CellPress
OPEN ACCESS

Cell

Article

Control of mammalian locomotion by ventral spinocerebellar tract neurons

Joshua I. Chalif,[1,2,5] María de Lourdes Martínez-Silva,[1,2] John G. Pagiazitis,[1,2] Andrew J. Murray,[4] and George Z. Mentis[1,2,3,6,*]

[1]Center for Motor Neuron Biology and Disease, Columbia University, New York, NY 10032, USA
[2]Department of Neurology, Columbia University, New York, NY 10032, USA
[3]Department of Pathology and Cell Biology, Columbia University, New York, NY 10032, USA
[4]Sainsbury Wellcome Centre, University College London, 25 Howland Street, London W1T 4JG, UK
[5]Present address: Department of Neurosurgery, Brigham and Women's Hospital, Boston, MA 02115, USA
[6]Lead contact
*Correspondence: gzmentis@columbia.edu
https://doi.org/10.1016/j.cell.2021.12.014

SUMMARY

Locomotion is a complex behavior required for animal survival. Vertebrate locomotion depends on spinal interneurons termed the central pattern generator (CPG), which generates activity responsible for the alternation of flexor and extensor muscles and the left and right side of the body. It is unknown whether multiple or a single neuronal type is responsible for the control of mammalian locomotion. Here, we show that ventral spinocerebellar tract neurons (VSCTs) drive generation and maintenance of locomotor behavior in neonatal and adult mice. Using mouse genetics, physiological, anatomical, and behavioral assays, we demonstrate that VSCTs exhibit rhythmogenic properties and neuronal circuit connectivity consistent with their essential role in the locomotor CPG. Importantly, optogenetic activation and chemogenetic silencing reveals that VSCTs are necessary and sufficient for locomotion. These findings identify VSCTs as critical components for mammalian locomotion and provide a paradigm shift in our understanding of neural control of complex behaviors.

INTRODUCTION

Locomotion is an essential animal behavior that is critical for survival. Overground locomotion is defined as the alternating, rhythmic motor activity between opposing limbs, as well as between antagonistic muscles of the same limb. Although sensory feedback and supraspinal commands are important for modulating locomotion, a network of spinal interneurons—known as the central pattern generator (CPG)—is thought to be responsible for the genesis of locomotor activity (Guertin, 2012; Kiehn, 2016) without relying on sensory or descending inputs (Graham Brown, 1911). These neurons are thought to activate spinal motor neurons (MNs) in a patterned manner. Subsequently, MNs convey their motor commands to peripheral muscles, resulting in limb movement. Recent studies have begun to unravel the organization of the spinal neuronal circuits underlying left-right and flexor-extensor alternation (Crone et al., 2008; Gosgnach et al., 2006; Talpalar et al., 2013; Zhang et al., 2014), demonstrating the modularity and speed-dependency of these circuits. However, it is unknown whether a single neuronal population is necessary and sufficient for the generation and maintenance of locomotor activity. Here, using mice as an experimental model, we identify ventral spinocerebellar tract neurons (VSCTs) as an essential population of spinal neurons for mammalian locomotion.

In rodents, locomotor behavior is evident at early postnatal periods, since intact *ex vivo* spinal cord preparations can produce locomotor-like behavior following sensory fiber stimulation or application of a cocktail of drugs (Mentis et al., 2005; Talpalar et al., 2013; Whelan et al., 2000). This behavior is characterized by alternating rhythmic oscillations of MN activity between the left and right sides of the spinal cord and between rostral (L1/L2) and caudal (L4/L5) lumbar segments (Bonnot et al., 2002). Traditionally, CPG networks are thought to reside upstream of MNs (Goulding and Pfaff, 2005; Kiehn and Butt, 2003), whereas MNs act as the spinal output to convey motor commands to muscles. However, we have previously shown that stimulation of MN axons results in locomotor activity (Mentis et al., 2005). Additionally, manipulation of MN activity can alter ongoing locomotor behavior (Falgairolle et al., 2017) and zebrafish MNs can influence premotor excitatory CPG elements (Song et al., 2016). These observations implicate MNs in the regulation of locomotor rhythmogenesis via a local spinal neuron that is activated by MN axon collaterals. Although previous studies have provided evidence that the neural circuits encompassing CPG elements reside in the ventral spinal cord (Grillner and Wallén, 1985; Kiehn, 2016), the only spinal neurons that are contacted

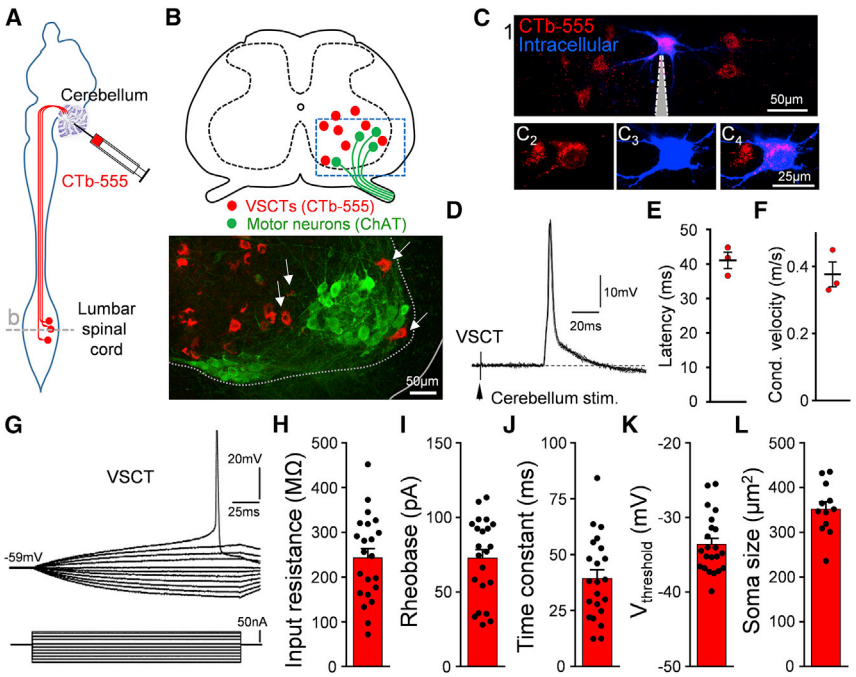

Figure 1. VSCTs located near or within the motor neuron nucleus are hyperexcitable

(A) CTb-555 injected in cerebellum at P0 to label VSCTs in the L1/L2 lumbar spinal cord.

(B) Drawing of the L2 spinal cord (dashed line in A) and confocal image from the ventral horn (box in drawing) showing VSCTs (red) near or within (arrows) MNs at P4 (ChAT; green) (N = 12).

(C) ($C_{1–4}$) Individual VSCTs (CTb-555; red) were visually targeted for intracellular recording (n = 22; N = 22 mice) using 2P-laser microscopy in the intact *ex vivo* spinal cord (intracellular dye: Cascade Blue Dextran). Gray: patch electrode.

(D) Five superimposed antidromic action potentials (APs) in a P3 L1 VSCT after cerebellum electrical stimulation at 1 Hz.

(E) Latency of antidromic APs for 3 VSCTs (N = 3).

(F) Conduction velocity.

(G) Superimposed traces from a current/voltage plot in a P4 L2 VSCT.

(H–L) VSCTs' input resistance (H) (n = 22), rheobase (I), time constant (J), threshold for induction of AP (K), and soma size (L) (n = 12). Data are represented as mean ± SEM. See also Figure S1.

by MN axon collaterals known to date are Renshaw cells (Alvarez and Fyffe, 2007; Eccles et al., 1954; Mentis et al., 2005; Renshaw, 1946) and Sim1$^+$ interneurons (Chopek et al., 2018). However, Renshaw cells do not affect the locomotor CPG (Enjin et al., 2017; Noga et al., 1987), and Sim1$^+$ neurons regulate the speed of vertebrate locomotion and contribute to vigor and coordination but are not involved in locomotor rhythmogenesis (Zhang et al., 2008). Thus, MNs may contact another yet-to-be-defined neuron that resides within the ventral spinal cord and mediates locomotor rhythmogenesis.

Here, we show that VSCTs are contacted by MN axon collaterals during early development via both chemical and electrical synapses. The nature of these contacts is both chemical via excitatory synapses, as well as electrical through gap junctions. Furthermore, VSCTs possess functional intrinsic properties consistent with a role in locomotor rhythmogenesis. We demonstrate that VSCTs contain axon collaterals that form local circuits with spinal MNs and at least Chx10$^+$ spinal neurons. Importantly, optogenetic activation and chemogenetic silencing of VSCTs reveals that VSCT neurons are both necessary and sufficient to produce locomotor behavior during postnatal development. Finally, chemogenetic silencing of VSCTs in freely moving adult mice perturbs their locomotor ability.

RESULTS

VSCTs are activated monosynaptically and electrically by motor neurons

To investigate whether spinal MNs activate a yet-unknown interneuron, we unbiasedly examined the activity of spinal neurons through two-photon (2P) calcium imaging in the intact *ex vivo* mouse spinal cord at postnatal day 4 (P4). Spinal neurons were indiscriminately labeled with calcium green 1 by electroporation (Figures S1A and S1B; STAR Methods). Stimulation of the ventral root (VR) revealed increases in fluorescence in interneurons located dorsolateral to the MN nucleus (Figures S1C and S1D). Visually guided, whole-cell, patch-clamp recordings revealed that these neurons displayed graded excitatory postsynaptic potentials (EPSPs) with a short latency following VR stimulation (Figure S1E), indicating that can be activated directly by MN axon collaterals. These neurons, located in the dorsal aspect of the MN nucleus were reminiscent of spinal border cells—a subset of VSCTs (Bras et al., 1988; Cooper and Sherrington, 1940). To determine whether these neurons were VSCTs, the tracer cholera toxin subunit b conjugated to Alexa-555 (CTb-555) was injected into the cerebellum in mice at P0 (Figure 1A). At P4, the injection was verified to be specific to the cerebellum (Figure S1F), as shown by CTb signal only in the cerebellum (Figure S1G). Individual VSCTs located in the L1/L2 spinal segments were then visually targeted for whole-cell patch-clamp recordings guided by 2P laser microscopy (Figures 1B and 1C) utilizing the *ex vivo* cerebellum-brainstem-spinal cord preparation. Only a single VSCT was recorded per spinal cord, targeted from the lateral aspect. In addition to co-localization of CTb-555 with the intracellular dye (Figure 1C), the identity of VSCTs was further demonstrated by the presence of an all-or-none antidromic action potential (AP) following cerebellum stimulation (Figures 1D–1F). VSCTs exhibited higher excitability compared with MNs (Fletcher et al., 2017; Figures 1G–1K) despite having a soma size similar to MNs (Fletcher et al., 2017; Figure 1L).

Next, we sought to identify the major source of synaptic activation of VSCTs. A major source of afferents originates from the periphery and sensory fiber stimulation can activate locomotor networks (Whelan et al., 2000). Thus, we tested whether dorsal

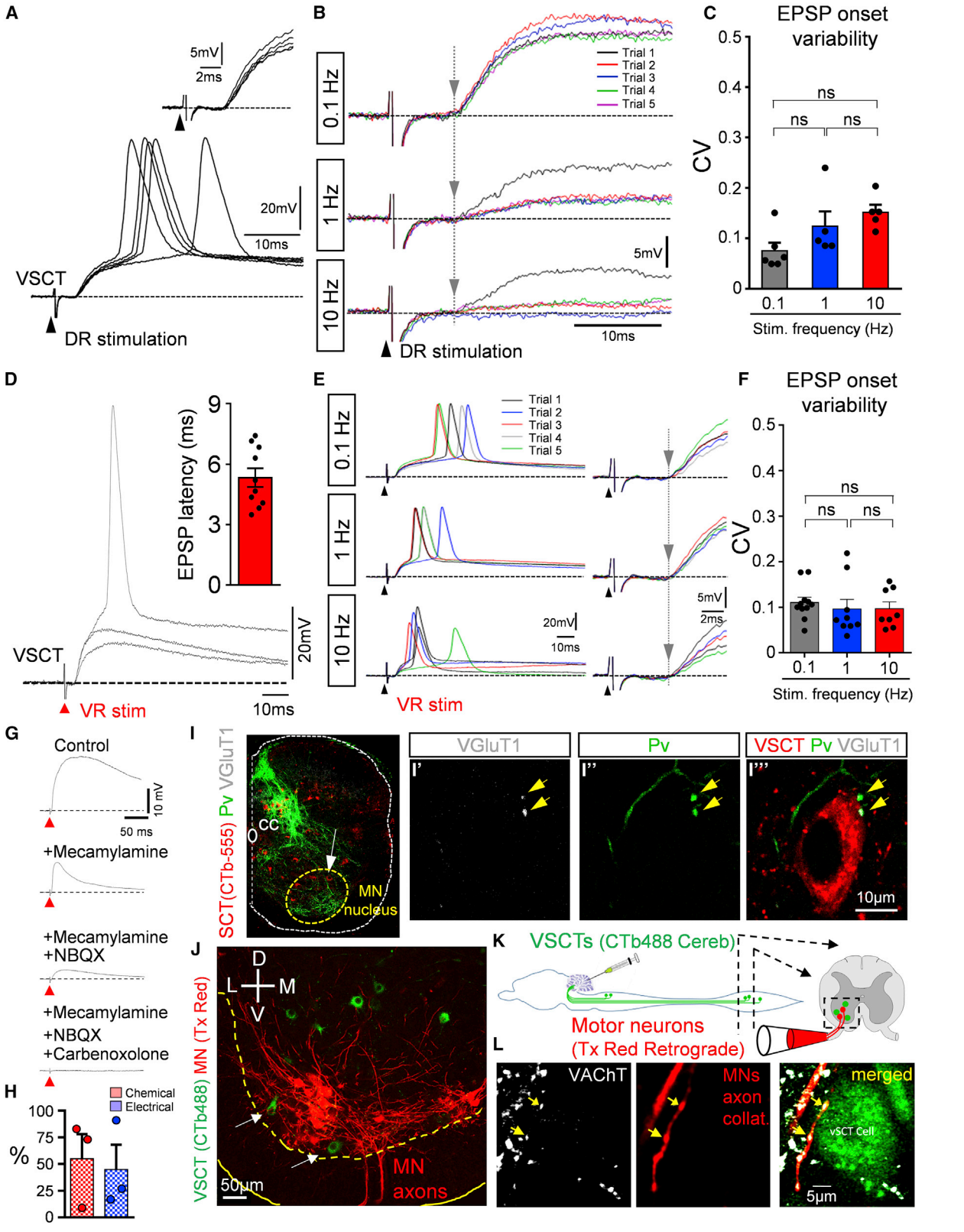

(legend on next page)

root (DR) stimulation, including proprioceptors, could activate VSCTs. Stimulation of the homosegmental DR revealed monosynaptically evoked EPSPs in 40% of VSCTs (6/15) at P3–P5 (Figure 2A). Monosynapticity was determined by the absence of a change in the coefficient of variation (CV) of the latency of the response onset at different stimulation frequencies (0.1–10 Hz) as we reported (Mendelsohn et al., 2015; Figures 2B and 2C). Staining with Parvalbumin (Pv) and vesicular glutamate transporter 1 (VGluT1) antibodies confirmed apposition of proprioceptive synapses on VSCTs (Figure 2I). To quantify the number of VSCTs receiving proprioceptive synapses, VSCTs were labeled with CTb-555 from cerebellum injection at birth. At P4/P5, DR L1 sensory fibers using the *ex vivo* spinal cord preparation were labeled orthogradely with Cascade Blue Dextran and subsequently marked with VGluT1 and Pv. The presence of VGluT1, Pv, and Dextran has been demonstrated to label selectively proprioceptive synapses (Chen et al., 2006; Mentis et al., 2006, 2011). We found that 8 VSCTs (~47%, 8/17, N = 6 mice) receive proprioceptive synapses on their soma or proximal dendrites (Figures S1H–S1J), whereas 9 VSCTs (~53%, 9/17, N = 6 mice) did not. These results are in agreement with our physiological studies and demonstrate that ~45% of VSCTs receive proprioceptive synapses.

Next, we examined whether VSCTs could be activated directly by MN axon collaterals. Utilizing the *ex vivo* spinal cord preparation (P3–P5), intracellular recordings of VSCTs (Figure 1C) exhibited short latency, depolarizing, and graded EPSPs sufficient to induce APs following VR stimulation (Figure 2D). All VSCTs (n = 10) were activated monosynaptically since different frequencies of VR stimulation (0.1–10 Hz) resulted in no change in the CV of the latency of the onset of EPSPs (Figures 2E and 2F). These EPSPs decreased at more depolarized holding potentials indicating the involvement of chemical synapses (Figures S1K and S1L). Through the addition of mecamylamine (cholinergic receptor blocker) and 2,3-dioxo-6-nitro-7-sulfamoyl-benzo[f]quinoxaline (NBQX) (glutamatergic receptor blocker), we determined that MNs activate VSCTs directly via both cholinergic and glutamatergic receptors (Figures 2G and 2H). Surprisingly, a residual component was evident following both cholinergic and glutamatergic blockade in VSCTs, which was blocked after exposure to carbenoxolone (gap junction blocker), indicating that MNs and VSCTs are also electrically coupled (Figures 2G and 2H). To evaluate the spread of current from the entire population of spinocerebellar tract neurons (SCTs) to a population of MNs located within one spinal segment, we utilized the cerebellum-brainstem-spinal cord *ex vivo* preparation at P4 and P5 (Figures S2A–S2C). Maximal cerebellum activation resulted in robust VR responses with a latency of ~40 ms (Figure S2C), consistent with the latency of the antidromic AP of VSCTs from the cerebellum (Figure 1E). Comparison of the VR response following cerebellar stimulation with that from the homonymous DR (Figures S2B and S2C) revealed that cerebellar stimulation resulted in ~35% of the MN activation compared with DR stimulation (Figures S2D and S2E). This indicates robust activation of MNs by axon collaterals from SCTs. The VR response was monosynaptic in nature since stimulation at different frequencies resulted in an identical latency, indicative of monosynapticity (Figure S2F). By measuring the VR response following cerebellum stimulation under carbenoxolone exposure (100 μM) we found a significant, yet modest, ~15% reduction of the VR response (Figures S2G and S2H). Further exposure to NBQX (20 μM) and amino-5-phosphonovaleric acid (APV) (100 μM) (non-NMDA and NMDA glutamate receptor blockers, respectively) abolished the VR response (Figures S2G and S2H). These results indicate that the spread of current through gaps junctions from SCTs to MNs is minimal and the chemical nature of communication between VSCTs and MNs is dominant.

The nature of MN-to-VSCT synaptic transmission was further investigated by morphological analysis in which MN axon collaterals were found to form cholinergic synapses on VSCTs (Figures 2J–2L). The electrical communication between VSCTs and MNs was also established morphologically. During intracellular recordings, Neurobiotin (in intracellular electrode) was allowed to diffuse into the recorded neuron as to reveal its somato-dendritic morphology and axonal trajectory. However, Neurobiotin is also a tracer known to cross gap junctions (Pastor et al., 2003) and identify dye-coupled partners of the recorded neuron. In this manner, we observed Neurobiotin-labeled MNs following a single VSCT fill (Figures S2I and S2J), and dye coupling was also observed among VSCTs (Figure S2K). Seven

Figure 2. VSCTs receive synapses from proprioceptors and motor neuron axon collaterals

(A) Superimposed responses from a P5 L1 VSCT after ipsilateral L1 dorsal root (DR) stimulation. Inset shows constant short latency responses.

(B) As in (A) from a P3 L2 VSCT after ipsilateral DR-L2 stimulation at 0.1, 1, and 10 Hz. Consecutive responses are color coded. Gray vertical line indicates constant latency of the response onset.

(C) Coefficient of variation (CV) of latency in the onset of EPSP in VSCTs after DR stimulation (ns: no significance; one-way ANOVA, Brown-Forsythe test).

(D) Superimposed graded EPSPs from a P4 L2 VSCT after ipsilateral homosegmental ventral root (VR) stimulation. Inset: latency of EPSPs in 10 VSCTs.

(E) As in (D) from a P4 L2 VSCT after ipsilateral VR-L2 stimulation at 0.1, 1, and 10 Hz. Traces on the right are expanded in time. Gray vertical line indicates constant latency.

(F) CV of the onset of EPSPs in VSCTs evoked by VR stimulation (one-way ANOVA).

(G) EPSP in a P4 L2 VSCT after ipsilateral VR stimulation in control solution, and sequential addition of mecamylamine (50 μM), NBQX (20 μM), and carbenoxolone (100 μM).

(H) Percentage of response in VSCTs due to chemical (red) and electrical (blue) transmission (n = 3 VSCTs, N = 3 mice).

(I) SCTs (CTb-555; red), Parvalbumin (green), and VGluT1 (white) immunoreactivity in L1 at P4 (n = 7). (I′–I‴) L1 proprioceptive fibers (Parvalbumin; green) and VGluT1$^+$ synapses (white; yellow arrows) onto a VSCT (red) shown by white arrow in (I).

(J) Ventral horn confocal image showing VSCTs (green) located close or within (arrows) the MN (red) nucleus.

(K) Protocol in which CTb-488 injected in cerebellum at P0 to label VSCTs (green). At P4, MNs were backfilled with Texas red dextran (red) from the VR using *ex vivo* spinal cord.

(L) Single-plane confocal images showing VAChT immunoreactivity (white), MN axon collaterals (red), and a VSCT (green), revealing two synapses (yellow arrows) (n = 7 VSCTs, N = 3 mice). Data are represented as mean ± SEM. See also Figures S1 and S2.

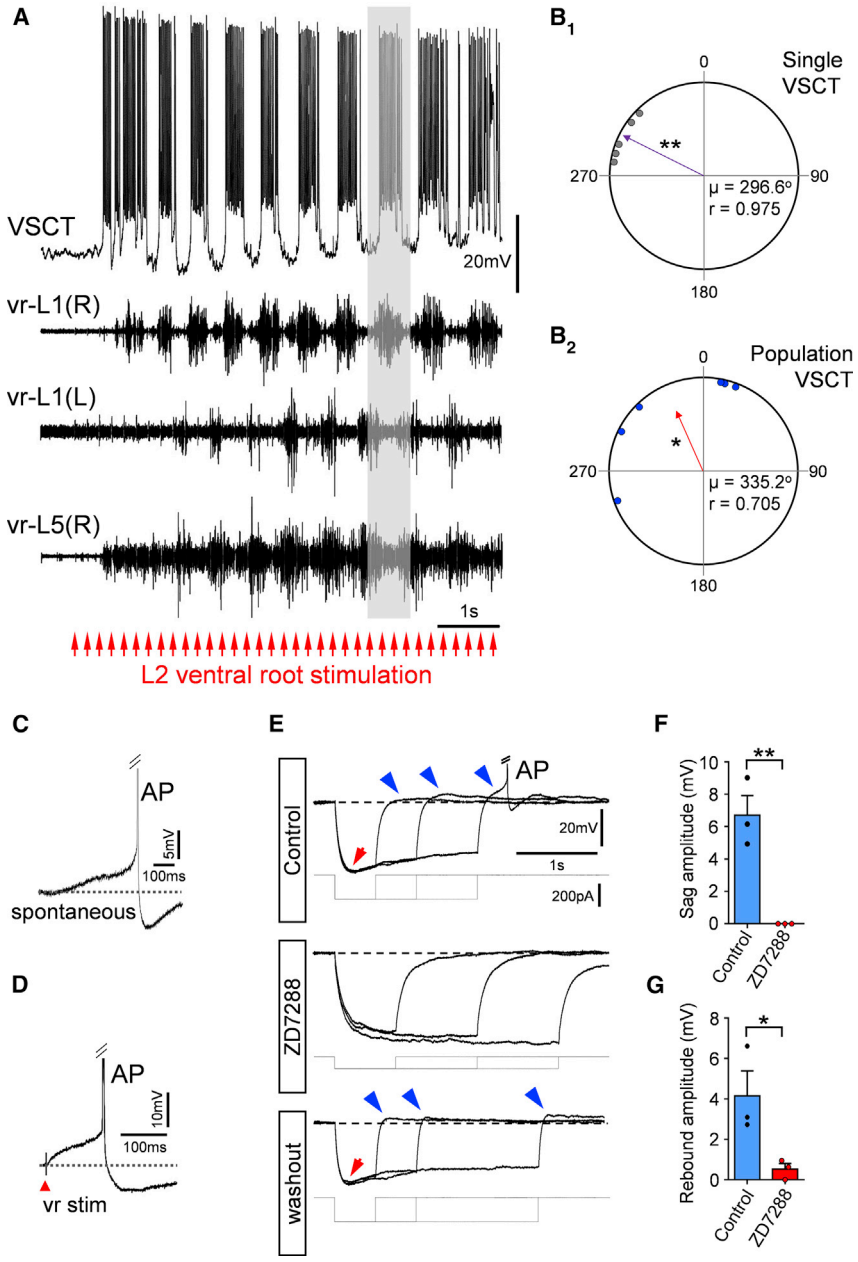

Figure 3. VSCTs are rhythmic during locomotor behavior and exhibit rhythmogenic properties

(A) Rhythmic activity in a P4 L1 VSCT together with filtered extracellular traces from ipsilateral (R) and contralateral (L) homosegmental L1 VRs and L5 (R) VR during locomotor-like activity induced by electrical stimulation of VR-L2 (bottom red arrows; 5 Hz for 10 s). Stimulus artifacts have been removed for clarity (n = 6 VSCTs, N = 6 mice).

(B) (B_1) Quantification of timing of first AP in a single VSCT with respect to the locomotor cycle in the homosegmental VR. Purple arrow vector indicates that the VSCT exhibited significant rhythmicity and fired prior to the onset of MN activity. **p < 0.01, Rayleigh test. (B_2) Quantification of timing of firing for the population of VSCTs to the locomotor cycle. Each data point represents the rhythmic vector value from individual VSCTs (purple arrow in B_1). Red arrow vector indicates that the population of VSCTs exhibit rhythmic activity preceding MN activity. * p < 0.05, Rayleigh test. μ, mean vector; r, length of the mean vector.

(C and D) VSCTs exhibit characteristics of a pacemaker current both spontaneously (C) and evoked after VR stimulation (D) (n = 6, N = 6).

(E) Superimposed voltage responses from a P4 L2 VSCT exhibiting a sag (red arrow) and post-inhibitory rebound (blue arrows) after negative current injection (bottom traces). Truncated AP is shown in (E). ZD7288 (100 μM) abolished both sag and post-inhibitory rebound and recovered after washout.

(F and G) Sag (F) and post-inhibitory rebound (G) amplitude before and after ZD7288 in 3 VSCTs. *p < 0.05, **p < 0.01; two-tailed Student's t test. Data are represented as mean ± SEM. See also Figure S3.

VSCTs (~60%, 7/12) were dye coupled, three of which exhibited dye coupling only among other VSCTs, whereas three more VSCTs exhibited dye coupling with both other VSCTs and MNs. One VSCT was dye coupled only with MNs. Despite dye coupling underestimates the extent of electrical coupling due to limitations in the time and diffusion rate of the tracer, our results indicate a substantial degree of electrical coupling (>60%) for VSCTs.

Taken together, these experiments demonstrate that MNs activate VSCTs via both chemical and electrical synapses. They also reveal the electrical communication among VSCTs themselves.

VSCTs are rhythmically active during locomotor-like behavior

Lundberg postulated that VSCTs relay information about the activity of spinal networks to the cerebellum (Lundberg, 1971). This hypothesis gained traction from experiments in adult cats demonstrating that the activity of VSCTs is rhythmically modulated during locomotion after deafferentation (Arshavsky et al., 1972). To test whether VSCTs are rhythmically active during locomotor behavior, we induced locomotor-like activity utilizing the intact *ex vivo* mouse spinal cord (from T4 to *cauda equina*) as previously reported (Bonnot et al., 2002; Jiang et al., 1999). Stimulation of lumbar VRs or DRs (Mentis et al., 2005) while recording intracellularly from individual VSCTs (located in the L1/L2 segments) concomitantly with the left and right L1 VRs and the right (or left) L5 VR. VSCTs (n = 6) displayed robust rhythmic behavior and bouts of APs (Figure 3A) in phase with the ipsilateral, homosegmental L1 VR (containing predominately flexor MNs). Two more VSCTs exhibited subthreshold rhythmic oscillations during sensory-induced locomotor behavior (n = 2; Figure S3A).

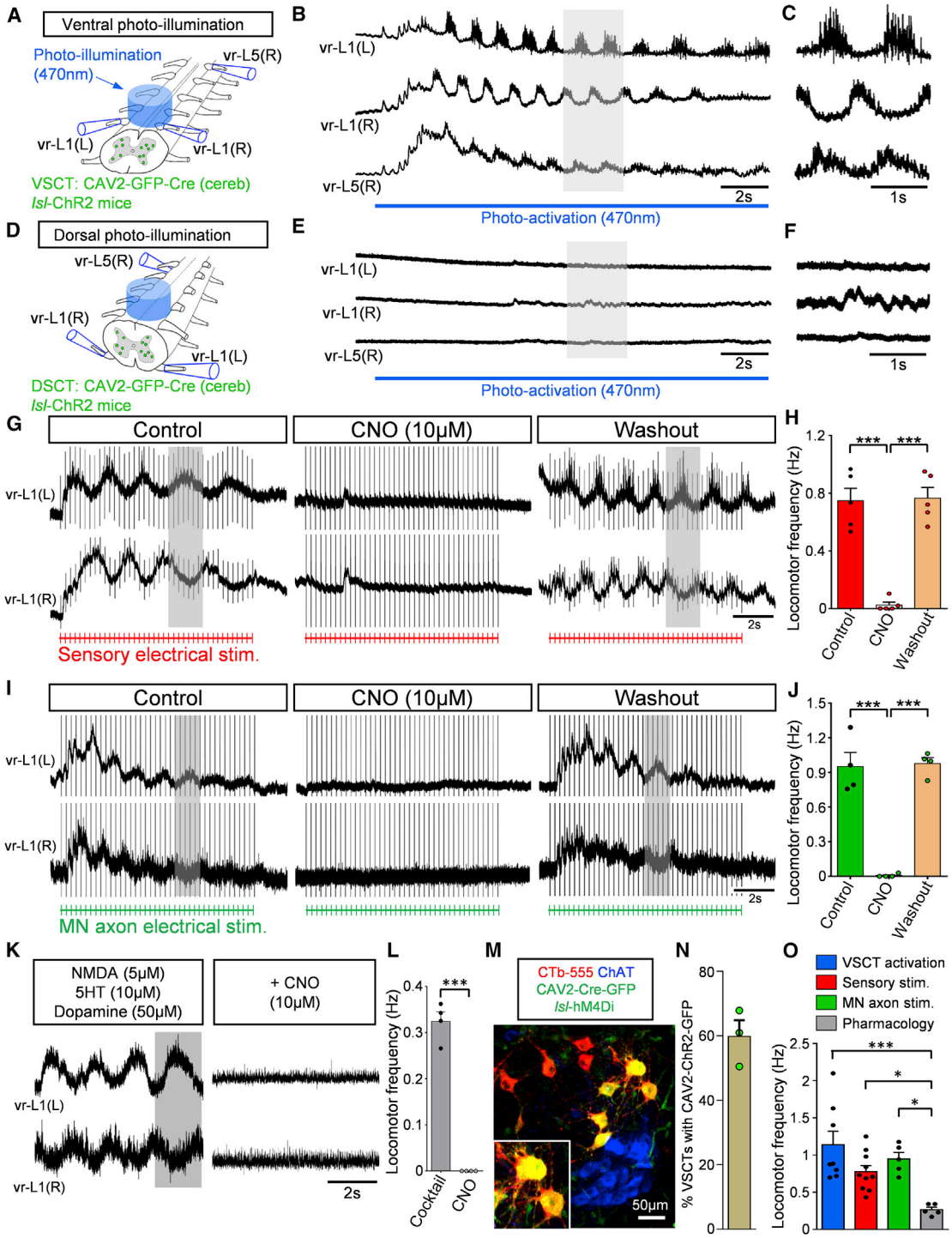

Figure 4. VSCTs are necessary and sufficient for locomotor-like behavior

(A and B) (A) Bilateral illumination with a 470 nm LED from the ventral aspect of L1 and L2 segments resulting in locomotor behavior recorded from L1 and L5 VRs (B) in *ex vivo* spinal cord at P4.

(C) Expanded traces (gray box in B) showing alternating activity between VRs (N = 8).

(D) Bilateral photoactivation of the dorsal aspect of the L1/L2 spinal cord.

(E) Extracellular VR responses following dorsal photoactivation (same spinal cord as in B but flipped over 180°).

(F) Time-expanded traces (gray box in E).

(legend continued on next page)

Calculation of the timing of the onset of VSCT firing compared with the onset of the flexor burst, normalized to the locomotor cycle length, revealed the relationship between the initiation of VSCT firing and that of MN firing in the same spinal segment for each locomotor cycle (Figure 3B$_1$; STAR Methods). The mean vector value from each of the individual VSCTs, plotted in a circular plot corresponding to the locomotor cycle (Figure 3B$_2$), determined if the combined population of VSCTs exhibited rhythmic activity. On average, we found that VSCTs elicited their first AP preceding the onset of the cycle from the homosegmental VR (Figures 3B$_1$, 3B$_2$, and S3B; STAR Methods). Thus, VSCTs fire rhythmically with flexor MNs and elicit APs prior to the locomotor cycle exhibited by homosegmental MNs.

VSCTs exhibit rhythmogenic characteristics

We observed that VSCTs exhibited a pacemaker current, a rhythmogenic property characterized by a slow, steady depolarization until the threshold voltage for AP induction is reached both spontaneously (Figure 3C) and evoked (Figure 3D). The H-current (I_h) is caused by the opening of a non-selective cation channel with an equilibrium potential of −35 mV and is known to underlie pacemaker currents in neurons (Lüthi and McCormick, 1998). VSCTs displayed the characteristic voltage sag and post-inhibitory rebound in response to a negative current injection, indicative of the presence of I_h (Figure 3E). The sag and post-inhibitory rebound were both time dependent and voltage dependent (Figures S3C and S3D). The post-inhibitory rebound was large enough to cause VSCTs to fire an AP from their own resting membrane potential (Figures 3E, S3C, and S3D). Both sag and post-inhibitory rebound were abolished by bath application of ZD7288—a selective blocker of I_h (Rothberg et al., 2002)—and recovered upon washout (Figures 3E–3G). ZD7288 decreased the resting membrane potential of VSCTs, increased their excitability, and did not affect the threshold voltage for AP induction (Figures S3E–S3J) as expected (Kase and Imoto, 2012; Lüthi and McCormick, 1998). Taken together, the electrical coupling between VSCTs and the presence of the pacemaker h-current may underlie the contribution of VSCTs to locomotor rhythmogenesis.

VSCTs are necessary and sufficient for locomotor rhythmogenesis during early postnatal development

To address the functional involvement of VSCTs in locomotor behavior, we used viral-mediated gene delivery to selectively manipulate neuronal activity of SCTs. Cerebellum injection with canine adenovirus 2 (CAV2) expressing GFP demonstrated effective and specific transduction of SCTs (Figure 4M). The efficiency of VSCTs transduction by CAV2-GFP-Cre was ∼60% (Figures 4N, S4A, and S4B) when compared with CTb-555 co-injected to cerebellum at P0/P1 and examined at P4/P5. To activate VSCTs, CAV2-GFP-Cre, CAV2-Cre, or CAV2-GFP was injected into the cerebellum of *lsl*-Channelrhodopsin2 mice at P0. We then used the *ex vivo* spinal cord preparation (T4-*cauda equina*) at P4 and 470 nm light—delivered through a LED—to photoactivate VSCTs bilaterally in the L1/L2 lumbar segments (Figure 4A), considered as the most rhythmogenic spinal cord area (Cazalets et al., 1995; Kjaerulff and Kiehn, 1996). Remarkably, VSCT photoactivation produced robust locomotor-like behavior in all preparations (N = 8) (Figures 4B and 4C). Dorsal spinocerebellar tract neurons' (DSCTs) illumination from the dorsal aspect in the same preparations (flipped over 180°, Figure 4D) revealed no effects (Figures 4E and 4F). The same preparations (N = 8) were flipped over once more to activate VSCTs, resulting in robust locomotor behavior and indicating that VSCTs, but not DSCTs, were responsible for locomotor behavior. Morphological experiments revealed the presence of ∼1,200 DSCTs (Figures S4C and S4D) and ∼850 VSCTs (Figures S4C and S4E) in the L1 spinal segment at P4. In control experiments, LED illumination had no effects on VSCTs expressing CAV2-GFP (Figures S4F–S4H). Using a distinct approach, ChR2 was introduced to SCTs by a rabies virus (N2C) expressing both ChR2 and YFP as previously reported (Reardon et al., 2016). The virus was injected into the cerebellum in wild-type (WT) mice at P0 and experiments were performed at P4 and P5 using the *ex vivo* spinal cord to photoactivate VSCTs from the ventral side with a 470 nm LED. This approach also produced robust locomotor-like activity with similar locomotor frequencies (Figures S5A–S5C) to those observed when CAV2-Cre injected in *lsl*-ChR2 mice. Importantly, the frequency of the induced locomotor rhythm following photoactivation of VSCTs was similar to that produced after sensory or MN axon stimulation and faster than that produced via application of a pharmacological cocktail (Figure 4O). Together, these results demonstrate that activation of VSCTs is sufficient to elicit locomotor behavior.

Archaerhodopsin-3 (ArchR3) was introduced to VSCTs by injection of CAV2-GFP-Cre (or CAV2-GFP) into the cerebellum of *lsl*-ArchR3 mice at P0 (Figure S5D) to silence VSCTs during

(G) Locomotor behavior evoked by sensory stimulation before, during, and after CNO washout in a spinal cord expressing hM4Di in VSCTs (duration of stimulation: red drawing at the bottom, 4 Hz for 10 s).
(H) Locomotor frequency after sensory stimulation before, during CNO and after washout (N = 5). (Control versus CNO: ***p < 0.001; CNO versus washout: ***p < 0.001, one-way ANOVA, Tukey's post hoc test.)
(I) As in (G), locomotor behavior induced following VR stimulation (bottom in green, 5 Hz for 10 s) before, during, and after CNO application.
(J) Locomotor frequency following MN axon stimulation before, during, and after CNO (N = 4). (Control versus CNO: ***p < 0.001; CNO versus washout: ***p < 0.001, one-way ANOVA, Tukey's post hoc test.)
(K) Similar to (G) and (I), VR responses in which locomotor activity was induced by application of NMDA (5 μM), 5 HT (10 μM), and dopamine (50 μM). Exposure to CNO abolished locomotor activity.
(L) Locomotor frequency evoked by pharmacological activation before and after CNO application (N = 4). ***p < 0.001, two-tailed Student's t test.
(M) Confocal image showing MNs (ChAT, blue), VSCTs (CTb-555, red), and CAV2-Cre-GFP (green) in a *lsl*-hM4Di mouse.
(N) Percentage of VSCTs transduced with CAV2-GFP at P5 (N = 3).
(O) Locomotor frequency under photoactivation of VSCTs (blue), sensory (red), MN stimulation (green), and cocktail of drugs (gray) (VSCT versus pharmacology: ***p < 0.001; sensory versus pharmacology, *p < 0.05; MN axon versus pharmacology, *p < 0.05, one-way ANOVA, Tukey's post hoc test). Data are represented as mean ± SEM. See also Figures S4 and S5.

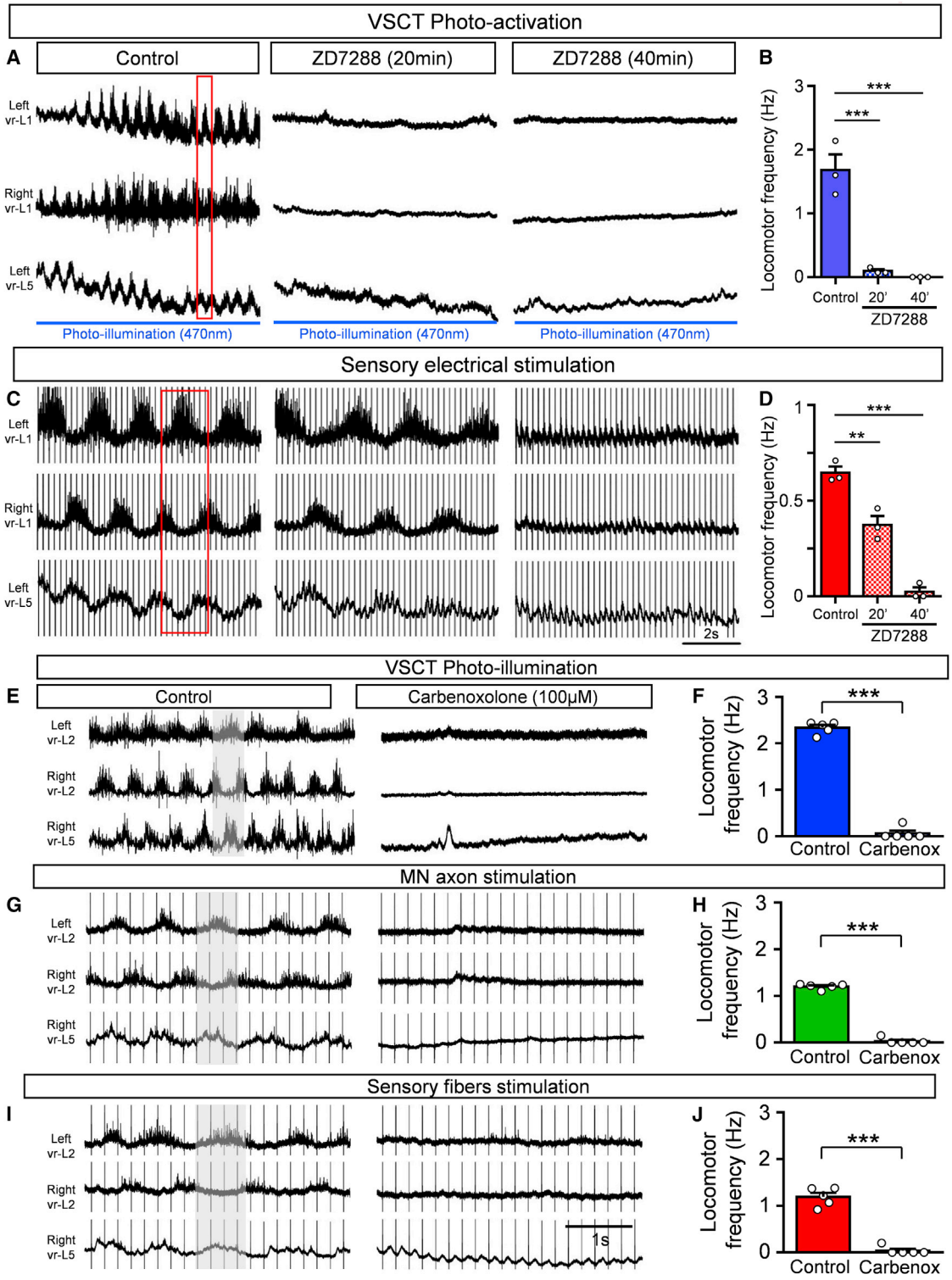

Figure 5. The locomotor activity induced after photoactivation of VSCTs depends upon the h-current and gap junctions

(A) Locomotor-like behavior induced by photo-illumination of VSCTs expressing ChR2 at P4 under control aCSF, and its abolition 20 and 40 min after 100 µM ZD7288 application. Duration of photoactivation: blue line. Red box: alternating activity in VRs.

(B) Locomotor frequency before, 20 and 40 min after ZD7288 (N = 3).

(C) Locomotor activity induced by sensory electrical stimulation in the same spinal cord shown in (A). Exposure to ZD7288 reduced locomotor activity after 20 min and abolished it after 40 min.

(legend continued on next page)

sensory-evoked locomotor activity to reveal whether VSCTs are necessary for locomotor behavior. Utilizing the *ex vivo* spinal cord preparation, we photo-silenced VSCTs through illumination with a 585 nm LED light delivered to the L1/L2 segments ventrally and bilaterally (Figures S5E and S5F) at P3–P5, which resulted in severe degradation of locomotor activity (Figures S5G and S5H). To increase the number of silenced VSCTs beyond those neurons located in L1/L2 segments, we next used a chemogenetic approach by injecting CAV2-GFP-Cre or CAV2-GFP at P0 into the cerebellum of mice with a floxed inhibitory designer receptor exclusively activated by designer drugs (DREADDs; hM4Di) (Figures 4M and 4N). Strikingly, bath application of clozapine N-oxide (CNO; 10 μM) to silence SCTs throughout the spinal cord prevented the induction of locomotor-like activity following either sensory stimulation (Figures 4G and 4H) or MN axon stimulation (Figures 4I and 4J). The effect was reversible because locomotor activity resumed ~30 min after CNO washout and following stimulation of either sensory fibers in a DR (Figure 4G) or MN axons in a VR (Figure 4I). Importantly, exposure to CNO did not affect glutamatergic neurotransmission as shown by the unchanged amplitude of the homosegmental monosynaptic DR-to-VR reflex (Figures S5I and S5J), indicating that MNs function normally. Exposure to CNO in mice injected with CAV2-GFP had no effect on the locomotor frequency induced by DR or VR stimulation as expected (Figures S5K and S5L). Thus, these experiments indicate that VSCTs are necessary for the induction of locomotor activity.

Silencing of SCTs through CNO exposure during ongoing locomotor-like activity induced by a cocktail of drugs (NMDA, serotonin, and dopamine) (Figures 4K and 4L), known to produce locomotor behavior in neonates (Bonnot et al., 2002; Mentis et al., 2005), abolished the activity shortly after CNO exposure, providing evidence that VSCTs are necessary not only for the induction of locomotor behavior but also for its maintenance (Figures 4K and 4L). In sum, these experiments demonstrate that VSCTs are necessary and sufficient to induce and maintain locomotor behavior during mouse development.

I_h current and electrical coupling in VSCTs mediate locomotor rhythmogenesis

Since VSCTs exhibit an I_h current, we investigated whether I_h is necessary to produce locomotor activity following photoactivation of VSCTs. This was compared side-by-side with locomotor activity induced by DR stimulation. VSCTs were transduced with by CAV2-GFP-Cre in *Isl*-ChR2 mice at P0. We then used a 470 nm light to photoactivate VSCTs bilaterally (from the ventral aspect) in the L1/L2 lumbar segments at P4 using the *ex vivo* spinal cord preparation. As we have shown before (Figure 4B), photoactivation of VSCTs resulted in robust locomotor-like activity (Figure 5A).

Bath application of ZD7288 (100 μM) abolished locomotor activity during VSCT photoactivation 20 min after exposure (Figures 5A and 5B) but in contrast, reduced the locomotor frequency by ~50% after sensory-induced locomotor activity (Figures 5C and 5D). However, locomotor behavior was abolished with both induction methods ~40 min after ZD7288 (Figures 5A–5D). These results demonstrate that the I_h current is a major contributor to the production of locomotor behavior during early development and that the channels responsible for the I_h in VSCTs play a prominent role in this behavior.

Since we established that VSCTs are electrically coupled with other VSCTs, as well as MNs, we next investigated the impact of electrical coupling in the production of locomotor behavior. The robust locomotor-like activity evoked at P3–P5 by photoactivation of L1/L2 VSCTs expressing ChR2 (after cerebellum injection with CAV2-GFP-Cre in *Isl*-ChR2 mice at P0) was abolished after ~40 min of carbenoxolone exposure (gap junction blocker [Mentis et al., 2005; Tresch and Kiehn, 2000]) (Figures S5M and S5N). Photoactivation of VSCTs in the L4/L5 segments also elicited robust locomotor activity that was subsequently abolished after addition of carbenoxolone demonstrating that activation of VSCTs in different lumbar segments also produces locomotor-like activity (Figures 5E and 5F).

Lastly, we tested the involvement of electrical coupling following electrically induced locomotor activity by stimulation of either MN axons (via VRs) or sensory fibers (via DRs) in the same spinal cord *ex vivo* preparations in which VSCTs were photo-activated. MN axon stimulation produced robust locomotor activity, whereas exposure to 100 μM carbenoxolone abolished this activity (Figures 5G and 5H). Similarly, DR stimulation resulted in locomotor activity of similar frequency to that produced by VR stimulation. Exposure to carbenoxolone abolished the locomotor behavior (Figures 5I and 5J). These results demonstrate that both I_h and electrical coupling contribute to the production of locomotor behavior following activation of VSCTs.

Circuit connectivity between VSCTs, motor neurons, and Chx10$^+$ spinal interneurons

To determine how VSCTs coordinate the production of locomotor behavior, we examined the circuit connectivity of VSCTs within the spinal cord by focusing on their outputs. We first sought to identify the neurotransmitter utilized by VSCTs marked by CTb-488 from cerebellum, using fluorescence *in situ* hybridization against the vesicular glutamate transporter 2 (VGluT2). Nearly all VSCTs (~93%, N = 3) express VGluT2 (Figures 6A and 6B), similar to DSCTs (~91%, N = 3) at P4. This result establishes that VSCTs are excitatory neurons, validating the proposal that SCTs are glutamatergic in nature (Atkinson et al., 2004).

VSCTs in the adult cat possess axon collaterals within the spinal cord (Bras et al., 1988). We used Neurobiotin to reveal the morphology of VSCTs that were intracellularly recorded and subsequently filled and found evidence of spinal axon collaterals in

(D) Locomotor frequency before, 20 and 40 min after ZD7288. **p < 0.01, ***p < 0.001, one-way ANOVA, Tukey's post hoc test for both (B) and (D).
(E–J) Locomotor activity induced by VSCT photoactivation in the L4/L5 segments from P3 and P4 mice (E) or MN axon (VR-L5 L) stimulation (G) or sensory fiber (DR-L5 L) stimulation (I) in the same spinal cord. Carbenoxolone (100 μM) abolished locomotor activity in all cases. Locomotor frequency following photoactivation of VSCTs (F), MN axon stimulation (H), and sensory fiber stimulation (J), before and after carbenoxolone. ***p < 0.001, two-tailed, unpaired t test (N = 5). Data are represented as mean ± SEM. See also Figure S5.

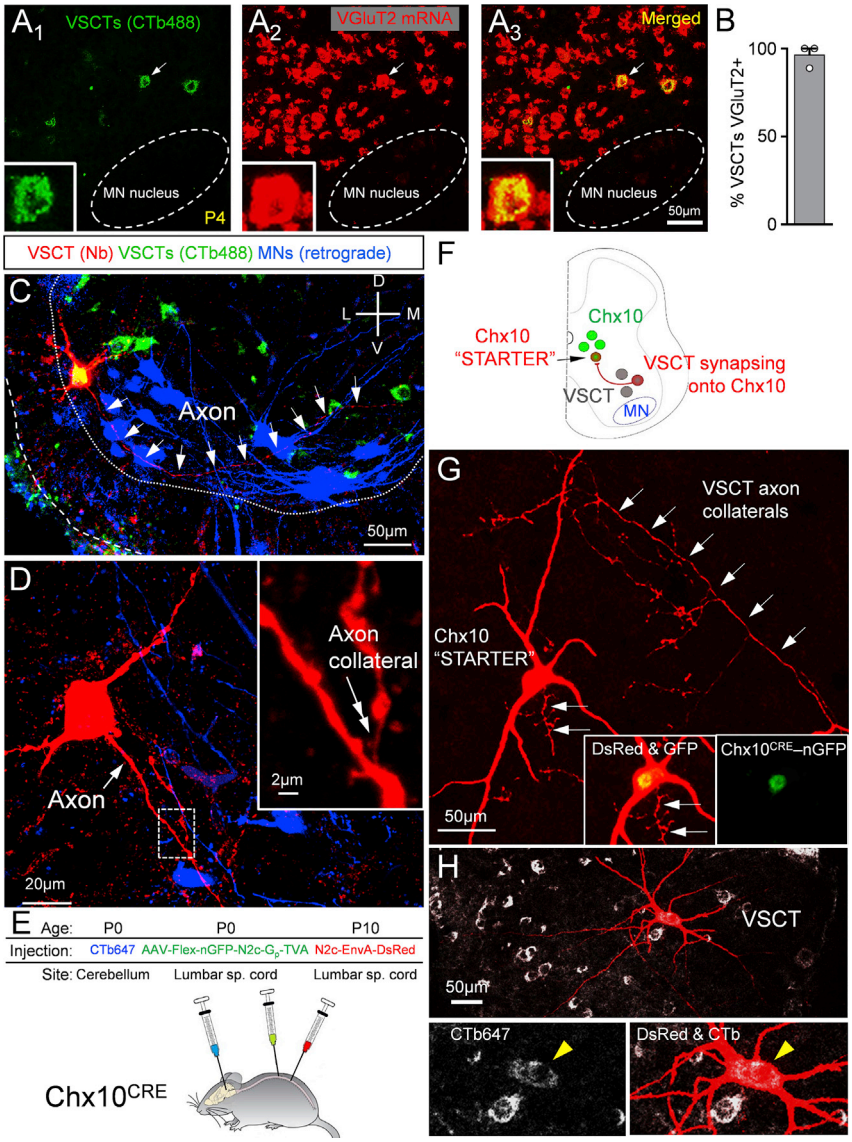

Figure 6. VSCTs are glutamatergic, possess spinal axon collaterals, and make synapses with Chx10 spinal neurons

(A) ($A_{1–3}$) VSCTs (CTb-488 from cerebellum, green) and VGluT2 mRNA (red) and merged image. Inset: VSCT (arrow in $A_{1–3}$) expressing VGluT2.

(B) Percentage of VSCTs expressing VGluT2 (N = 3).

(C) A P4 L2 VSCT filled with neurobiotin (red) after intracellular recording co-localizing with CTb-488 (cerebellum at P0). MNs were backfilled with a dextran dye from the VR (blue). White arrows mark VSCT axon.

(D) Higher mag of VSCT (in C), showing its main axon (white arrow) and an ipsilaterally projecting axon collateral (inset, double arrow; magnified from the dotted box).

(E) AAV2/1-Flex-nGFP-N2c-Gp-TVA injected in spinal cord at P0 to introduce the rabies G protein to Chx10 neurons ($Chx10^{Cre}$ mice). Concurrently, CTb-647 injected in cerebellum to mark VSCTs. Rabies-N2c-EnvA-dsRed was injected in spinal cord at P10.

(F) The "starter" Chx10 neurons are labeled with nuclear GFP and cytoplasmic dsRed. Neurons providing monosynaptic input to "starter" neurons are labeled with dsRed but not nGFP. VSCTs are identified through CTb-647.

(G) A Chx10 "starter" neuron identified by co-localization of dsRed and nGFP (insets). Arrows indicate VSCT axon collaterals synapsing onto the Chx10 "starter" neuron.

(H) VSCT (yellow arrowhead in insets) labeled by transynaptic transfection of its axon collaterals onto the Chx10 neuron. Data are represented as mean ± SEM. See also Figures S6 and S7.

neonatal VSCTs projecting both ipsilaterally and contralaterally to the VSCT soma (Figures 6C, 6D, and S6A–S6C). To investigate the presence of axon collaterals in a larger number of VSCTs, we first injected CTb-647 together with CAV2-Cre virus into the cerebellum of newborn mice and then injected AAV9-CBh-DiO-eGFP (Adeno-associate virus [AAV] carrying a flexed reporter) directly into the lumbar spinal segments a few days later (~P5–P7) to transduce VSCTs and ultimately visualize their axon collaterals (Figure S6D). The efficiency of the AAV9-CBh-DiO-eGFP to label VSCTs was relatively low, allowing to reveal the full somatodendritic and axonal trajectory in individual VSCTs (Figure S6E). We used Neurolucida to reconstruct VSCTs that possess axon collaterals (Figures S6F–S6H), and the identity of the axon and its collaterals was verified by ankyrin G (AnkG) (axonal marker) immunoreactivity in some VSCTs (Figures S6I and S6J). We observed axon collaterals in seven VSCTs (53%, 7/13). In six additional VSCTs, we did not observe axon collaterals along the visible length of the main axon, although they may contain axon collaterals at different spinal segments. Overall, these experiments indicate that ~55% of VSCTs possess axon collaterals.

To reveal the territory of synapses from axon collaterals of SCTs, we marked synapses from SCT axon collaterals within the L1/L2 lumbar segments, by co-localization of CTb-488 (cerebellum injection at P0), together with Synaptophysin and VGluT2 immunoreactivity at P5 (Figures S7A–S7D, N = 4), using single-plane confocal images and ImageJ analysis (see STAR Methods). These synapses were located medially in the intermediate gray matter and within the MN nucleus, whereas very few synapses were found in the lateral aspect of the intermediate gray matter or the dorsal horn (Figure S7D).

We also found that VSCTs directly contact ipsilateral and contralateral MNs (Figures S7E and S7F), as well as spinal interneurons, since VSCT axon collaterals were observed in the intermediate gray matter. To uncover the identity of the spinal interneurons contacted by VSCT axon collaterals, we investigated whether VSCTs synapse with $Chx10^{+}$ spinal neurons. We used a rabies (N2c) virus engineered to cross a single synapse in a retrograde fashion to identify neurons monosynaptically connected to a "starter" population (Reardon et al.,

2016), in this case Chx10$^+$ neurons. We injected Cre-conditional AAVs into the spinal cord of Chx10-Cre mice to restrict rabies glycoprotein (G) and TVA to Chx10$^+$ neurons (Figures 6E and 6F). Concurrently, we injected CTb-647 into the cerebellum to -label VSCTs. After ~10 days, we injected Rabies-N2c-EnvA-dsRed into the spinal lumbar segments. This virus, directly infects only Chx10$^+$ neurons and presynaptic neurons. Accordingly, the Chx10$^+$ "starter" population was labeled with a nuclear GFP (nGFP) and dsRed in the cytoplasm, whereas cells providing monosynaptic input to the starter population were labeled with dsRed only. Morphological analysis revealed one or more VSCTs (CTb$^+$ and ventral horn location) that were monosynaptically connected to Chx10$^+$ neurons (Figures 6G and 6H). These experiments indicated that VSCTs target Chx10$^+$ spinal neurons, as well as MNs. Importantly, they also showed morphological evidence of VSCT axon collaterals forming synapses with the soma and dendrites of Chx10$^+$ neurons in adult mice (Figure 6G, arrows).

Next, we investigated the extent of the VSCT axon collaterals' projection within the spinal cord by injecting two different CTb fluorescent tracers into the cerebellum and the L5/L6 caudal lumbar spinal cord segments at birth (Figure S7G). At ~P5, we examined the L1/L2 segments for VSCTs that expressed both fluorescent tracers. We found that ~34% of the L1/L2 VSCTs were double labeled (Figures S7H and S7I), demonstrating that VSCTs send descending axon collaterals to caudal spinal segments in addition to their main ascending axon to the cerebellum. Thus, VSCTs form local and extra-segmental spinal circuits with MNs, Chx10$^+$ neurons and likely with other spinal neurons via their axon collaterals.

Silencing SCTs in adult mice perturbs locomotor behavior

To investigate whether SCTs are essential for mammalian locomotor behavior in adult mice, we chemogenetically silenced SCTs in freely moving adult (P35–P45) mice. We first investigated whether there are any direct connections from the cerebellum to the spinal cord in mice as previously postulated in cats (Matsushita and Hosoya, 1978), rats (Bentivoglio and Kuypers, 1982), and mice (Sathyamurthy et al., 2020) by injecting CTb-555 in the L2/L3 spinal cord *in vivo* at P0 or P21 and examined the cerebellum at P4 and P35, respectively. We found no evidence of CTb-555 labeled neurons in the deep cerebellar nuclei either at P4 (Figures S8A–S8E) or at P35 (Figures S8F–S8J), indicating the lack of direct connections from the cerebellum to the lumbar spinal cord at these ages. To further exclude any potential effects of cerebello-spinal connections that might have been missed by CTb retrograde labeling, we used Cdx2^{FlpO} mice crossed with *fsf-lsl*-h4MDi mice to generate Cdx2^{FlpO}::*fsf-lsl*-h4MDi mice. In this way, we excluded not only any potential direct connections between cerebellum and spinal cord but also any effects of brain neurons possibly transduced from the cerebellum injections, thus limiting the expression of h4MDi to SCTs only, as Cdx2 is solely expressed in spinal cord (Abraira et al., 2017).

CAV2-GFP-Cre or CAV2-GFP or CTb-647 (for counting neurons) was injected into the cerebellum of Cdx2^{FlpO}::*fsf-lsl*-h4MDi mice at P21 (Figure 7A) and experiments performed at P35–P45, resulting in ~750 CTb-647$^+$ VSCTs in the L1 segment (Figures 7B and 7C; STAR Methods). We then counted the number of VSCTs in the L1 segment expressing GFP and found that ~400 VSCTs were transduced with CAV2-GFP-Cre (Figures 7D$_1$–7D$_3$ and 7E), which corresponds to a ~53% transduction efficiency comparable with that in neonates (Figure 4N). Expression of DREADDs within VSCTs was confirmed by immunoreactivity against the hemagglutinin (HA) tag co-localizing with CTb-647-labeled spinal neurons from the injected cerebellum (Figure S9A). Importantly, no HA immunoreactivity was observed in the cerebellum (Figure S9B), hippocampus (Figure S9C), cortex (Figure S9D), and brainstem (Figure S9E). In addition, selective Cdx2 expression throughout the spinal cord was confirmed by detecting mCherry fluorescence (Figure S9F). GFP$^+$ SCTs were found in the cervical (Figure S9G), thoracic (Figure S9H), and caudal lumbar (Figure S9I) spinal segments. Thus, only SCTs expressed the inhibitory DREADD receptors, ruling out any contributions from the brain during exposure to CNO.

Mice injected at P21 with CAV2-GFP-Cre (or CAV2-GFP) were injected with CNO (5 mg/kg, i.p.) at P35–P45 to silence SCTs. To assess quantitatively the locomotor ability of freely moving mice, we utilized the open field assay and measured the distance traveled for 10 min every hour for a total of 6 h. At the onset of the experiment (first 10 min following CNO injection) there was no statistical difference between CAV2-GFP-Cre and CAV2-GFP groups (Figures 7F$_1$ and 7G). Mice in the CAV2-GFP-Cre group revealed a progressive reduction in the distance traveled at 1 h post CNO injection compared with the controls (Figure 7G). Strikingly, the majority of mice in the CAV2-GFP-Cre group stopped moving between 2 and 3 h post CNO injection (Figures 7F$_2$, 7G, S9J, and S9K). As expected, the effects of CNO declined 4 h after CNO injection, and CAV2-GFP-Cre mice started moving around again (Figures 7G, S9J, and S9K).

To investigate further the locomotor ability of adult mice in which SCTs were "silenced," we used a swim test as a proxy for the locomotor CPG. Adult mice (~P35–P45) in which SCTs were chemically "silenced" by exposure to CNO were tested during free swimming. Cdx2^{FlpO}::*fsf-lsl*-h4MDi injected with either CAV2-GFP or CAV2-Cre were examined just prior to 10 mg/kg (equivalent dose to *ex vivo* experiments) CNO injection and 3 h after CNO injection, which we determined to be the optimal time point for the effect of CNO. High-speed videography was used in mice freely swimming for 30 s. We found that there was no statistical difference in the ability and total swim period between the two groups before CNO administration (Figure 7H). In striking contrast, mice that received CAV2-Cre cerebellum injections exhibited a strong reduction in their ability to swim 3 h after CNO administration (Videos S1A [pre-CNO], S1B [3 h CNO] for mouse A, S2A [pre-CNO], and S2B [3 h CNO] for mouse B). These mice exhibited a "floating" behavior during which their overall inability to swim was interspersed with short periods of swimming (Figure 7H; Videos S1 and S2). Control mice were able to swim for the entire testing period after 3 h from CNO administration (Figure 7H; Videos S3A [Pre-CNO] and S3B [3 h CNO] for mouse C), indicating that CNO itself did not have any effects on swimming behavior. The total period that mice were able to swim was significantly reduced in mice injected with CAV2-Cre (Figure 7H). Quantification of the

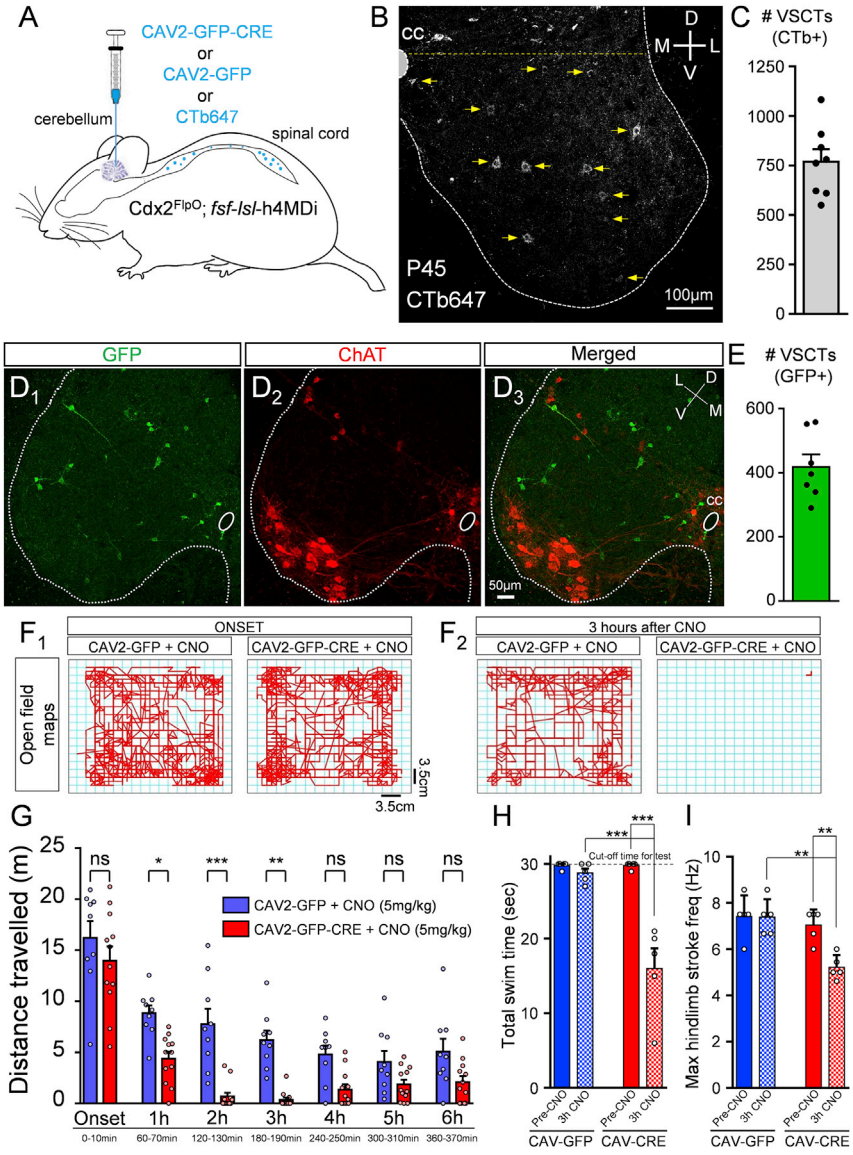

Figure 7. Silencing VSCTs *in vivo* in freely moving adult mice perturbs locomotor ability

(A) CAV2-GFP-Cre or CAV2-GFP or CTb-647 (for counting) was injected in cerebellum at ~P21 in Cdx2^{FlpO}::*fsf-lsl*-h4MDi mice.

(B) CTb-647^{+} neurons in the L1 segment in a P45 mouse. Neurons ventral to the yellow dotted line were defined as VSCTs.

(C and D) (C) Total number of VSCTs labeled with CTb-647 in the L1 segment (N = 8). GFP in the L1 segment (D_1: green), ChAT (D_2: red), and merged image (D_3).

(E and F) (E) Total number of GFP^{+} VSCTs in mice injected with CAV2-GFP-Cre (N = 7). Maps of distance traveled by a mouse in open field assay in 10 min at the onset (F_1) and 3 h (F_2) after 5 mg/kg CNO in mice injected with CAV2-GFP or CAV2-GFP-Cre. The same mouse is shown at the onset (F_1) and after 3 h (F_2) for each group (age: P45).

(G) Distance traveled by mice in bins of 10 min duration for each hour after CNO injection (N = 9 CAV2-GFP mice, blue; and N = 12 CAV2-GFP-Cre mice, red). Each point represents a single mouse. ns: no significance ($p > 0.05$), *$p < 0.05$, ***$p < 0.001$, one-way ANOVA, Tukey's post hoc test.

(H) Total swim time for control (CAV2-GFP; blue) and CAV2-Cre (red) mice, before (pre-CNO) and 3 h after 10 mg/kg CNO (3 h CNO).

(I) Maximum hindlimb stroke frequency during periods of swimming for the two groups. **$p < 0.01$, ***$p < 0.001$, one-way ANOVA, Tukey's post hoc test for both (H) and (I). Data are represented as mean ± SEM. See also Figures S8 and S9 and Videos S1, S2, and S3.

maximum hindlimb stroke frequency revealed that mice in the CAV2-Cre group displayed significantly lower maximum frequency compared with controls during the short periods in which they were able to swim (Figure 7I). Taken together, our experiments demonstrate that mice with "silenced" SCTs have significantly compromised ability to produce locomotor activity during both early postnatal development and in adulthood, pointing to VSCTs as essential drivers of mammalian locomotion.

DISCUSSION

Our discovery that VSCTs are core components of the CPG that are both necessary and sufficient for locomotor behavior represents a paradigm shift in our understanding of the mechanisms of locomotion. Instead of a distributed network responsible for locomotion, the neural control of locomotion may use VSCTs as a nodal point. Sensory inputs and descending supraspinal pathways (Baldissera and Roberts, 1975; Jankowska et al., 2011; Shakya Shrestha et al., 2012; Shrestha et al., 2012), as well as MN input (Falgairolle et al., 2017; Mentis et al., 2005), are all known pathways that initiate or regulate locomotion and converge on VSCTs. Our findings identify an unexpected function for VSCTs as key controllers of mammalian locomotion and demonstrate that a single neuronal type is essential for such behavior, fundamentally changing the way we think complex behaviors are produced.

Although the initiation of vertebrate locomotion takes place in the brain (Garcia-Rill, 1986; Jordan et al., 2008), and neurons in the brainstem can halt locomotion (Bouvier et al., 2015), the rhythm and pattern generation is solely produced by spinal neurons known as the locomotor CPG (Grillner, 2003; Kiehn, 2006). Several types of excitatory interneurons originating from some progenitor domains (V0, V2, and V3) have been proposed as putative rhythm generators (Gosgnach et al., 2017; Kiehn, 2016; Ziskind-Conhaim and Hochman, 2017). However, none of these interneurons is by itself necessary and sufficient for rhythm generation, which has led to the current view that rhythm generation

is not mediated by a single, homogeneous group of excitatory neurons (Kiehn, 2016).

Our study challenges this hypothesis and proposes that a single neuronal type initiates the locomotor CPG by demonstrating the necessity and sufficiency of VSCTs to produce locomotor activity. VSCTs are glutamatergic, project ipsilaterally, as well as contralaterally, and possess both intra- and inter-segmental axon collaterals making contacts with MNs, Chx10$^+$ spinal neurons and likely other spinal neurons.

The CPG is active at birth and has been under investigations for decades utilizing the neonatal *ex vivo* spinal cord as an experimental system. By providing exceptional accessibility to the activity and function of CPG neurons, this approach combined with mouse genetics and physiological and anatomical assays has transformed our capabilities to unravel the organization of the locomotor CPG (Jiang et al., 1999; Kiehn, 2016; O'Donovan et al., 2010; Smith and Feldman, 1987; Ziskind-Conhaim et al., 2010). Activation of VGluT2$^+$ neurons was shown to induce locomotor-like activity in neonates (Hägglund et al., 2010). However, Sim1$^+$ (Zhang et al., 2008) and Chx10$^+$ (Crone et al., 2008) neurons, both of which are VGluT2$^+$, were found to play a role in left-right coordination only (Ziskind-Conhaim and Hochman, 2017). In contrast, our findings show that VSCTs are VGluT2$^+$ neurons essential for the induction of locomotor behavior.

Locomotor-like activity can be evoked by sensory stimulation (Bonnot et al., 2002; Lev-Tov et al., 2000), exposure to pharmacological substances (Bonnot et al., 2002; Cazalets et al., 1995; Kjaerulff and Kiehn, 1996), and stimulation of MN axons (Mentis et al., 2005). The latter is considered a puzzling observation, since MNs are thought to act solely as the mediators of central commands to skeletal muscles. However, MNs have recently been proposed to provide feedback to the CPG during locomotor activity (Falgairolle et al., 2017; Song et al., 2016). Together, these observations raised the possibility that MNs may contact a yet-unknown interneuron that is key for the locomotor CPG. However, silencing of Renshaw cells and Sim1$^+$ interneurons, which are the only spinal interneurons contacted by MN axon collaterals known to date, did not affect locomotor rhythmogenesis (Enjin et al., 2017; Zhang et al., 2008). Our identification of VSCTs as a target of MN axon collaterals provides an answer to this conundrum. VSCTs receive monosynaptic activation from MNs that is both cholinergic and glutamatergic in nature, consistent with previous findings that spinal MNs axon collaterals release both acetylcholine and glutamate or aspartate (Mentis et al., 2005; Nishimaru et al., 2005; Richards et al., 2014). These observations point to a positive feedback neuronal circuit between MNs and VSCTs that enables early, robust activation of VSCTs and subsequent activation of other neurons involved in locomotor behavior.

We also discovered that VSCTs are electrically coupled among themselves. What is the importance of this electrical coupling in the context of locomotor rhythmogenesis? In the developing mammalian spinal cord, locomotor-like rhythm generation can be produced solely through gap junctions (Tresch and Kiehn, 2000). We propose that gap junctions among VSCTs are critical for the induction of locomotor rhythmogenesis. Accordingly, we reveal that gap junction blockade using carbenoxolone abolishes locomotor behavior induced in neonates by (1) direct photoactivation of VSCTs, (2) sensory stimulation, or (3) MN axon stimulation. Electrical communication among spinal neurons is thought to be an important circuit mechanism in the locomotor CPG (Ziskind-Conhaim and Hochman, 2017), and we argue that a key function of electrical coupling among VSCTs is to synchronize their activity. In addition, chemical neurotransmission may not be necessary for the production of rhythmic output across the rostro-caudal axis since photoactivation of VSCTs in either the rostral (L1/L2) or the caudal (L4/L5) spinal segments resulted in robust locomotor activity.

Intriguingly, some VSCTs also communicate electrically with MNs via gap junctions. Neonatal mammalian MNs are electrically coupled among themselves only during the first two postnatal weeks (Chang et al., 1999; Mentis et al., 2002; Personius et al., 2007; Walton and Navarrete, 1991). Our findings that VSCTs are electrically coupled with a subset of MNs indicate that electrical coupling is not selective among a single neuronal type. Moreover, an important implication of these findings is that depending on the extent and strength of coupling, the phase change in their respective membrane potential during the locomotor behavior will be similar and likely contribute to the recruitment of VSCTs, as well as the neuronal targets of their axon collaterals.

The observation that VSCTs possess rhythmogenic properties provides additional mechanistic support to their function as essential neurons for locomotor rhythmogenesis. VSCTs possess the I_h current that has been previously implicated as a key cellular property in rhythmic behaviors, such as in the inspiratory pre-Bötzinger complex neurons in mice (Thoby-Brisson et al., 2000) or in the rhythmic behavior of pyloric neurons of the stomato-gastric ganglion in lobsters (Zhang et al., 2003). I_h is strongly activated by hyperpolarization (Pape, 1996), as well as in a time- and voltage-dependent membrane conductance. Although the precise role of I_h in VSCTs during locomotor activity remains to be elucidated, it is possible that I_h may limit the effect of rhythmic inhibition and cause the membrane potential to escape more rapidly from inhibition during locomotor activity. In addition, since I_h regulates the post-inhibitory rebound potential and neuronal excitability, I_h may also be involved in the acceleration of the arrival of the first AP and thus contribute to the enhanced recruitment of VSCTs. Finally, in tadpoles I_h has been shown to mask an ultraslow AHP generated by sodium-potassium pumps that would normally inhibit activity (Picton et al., 2018); therefore, the presence of I_h may also influence the excitability state of VSCTs.

VSCTs were first discovered by Cooper and Sherrington (1940) and have been hypothesized to serve as "efferent copies" of spinal motor networks (Lundberg, 1971), whereby they provide the cerebellum with feedback information regarding the ongoing state of the ventral spinal cord. During repetitive motor tasks, like locomotion or scratching, signals from the spinal CPG evoke rhythmic activity in the cerebellar cortex whose outputs modulate the descending tracts that regulate the spinal rhythmic activity (Grillner and Wallén, 1985; Martínez-Silva et al., 2014; Morton and Bastian, 2003; Rand et al., 1998). The cerebellum-brainstem-spinal cord loop is essential for coordinated and adaptive gait control. However, the cerebellum is not critical to generate locomotion, rather it modulates limb movement patterns, balance, and adaptation (Hammar et al., 2011; Pisotta and

Molinari, 2014). Our findings that VSCTs are essential for the initiation and maintenance of locomotion imply that VSCTs are not purely a relay messenger of information as originally proposed. Instead, in addition to their role in coordinating locomotion at the spinal level, VSCT output to the cerebellum may be critical for the regulation of locomotion by the cerebellum and other supraspinal areas influenced by cerebellar output. To this end, and although the precise neuronal circuit mechanisms involving VSCTs in adult locomotion remain to be elucidated, our observations that Chx10^{+} spinal neurons are synaptic targets of VSCT axon collaterals in adults provides a potential insight. Chx10^{+} spinal neurons are known to be activated during adult locomotion (Al-Mosawie et al., 2007) and have been shown to function in the maintenance of locomotor rhythmicity and in left-right alternation (Crone et al., 2008, 2009). Thus, we suggest that Chx10^{+} spinal neurons receive significant activation by VSCTs during adult locomotion and without which the animal's locomotor ability is significantly compromised. The importance of the spinal axon collaterals of VSCTs versus their main ascending axon to the cerebellum for the induction of locomotor behavior is underscored by observations in which *in vivo* adult spinalized mice were able to produce fictive locomotion (Meehan et al., 2012, 2017). In addition, cerebellectomy has been shown to have little impact on the ability of other organisms to locomote, including fish (Roberts et al., 1992), rats (Federico et al., 2006), cats (Udo et al., 1980), monkeys (Wirth and O'Leary, 1974), as well as in humans either due to cerebellum agenesis or cerebellar resection due to tumors (Earhart and Bastian, 2001; Ilg et al., 2008; Yu et al., 2015).

In conclusion, we discovered that VSCTs are both necessary and sufficient for locomotor behavior and that they are core components of the locomotor CPG. It also provides the conceptual foundation for developing therapeutic approaches for patients suffering from spinal cord injury and motor disorders.

Limitations of the study

One limitation of our study is that we cannot fully exclude the potential involvement of DSCTs in locomotor behavior in adult mice as we demonstrated in neonatal mice. The optogenetic approaches used in neonates cannot be employed in adult mice for technical reasons. However, DSCTs, including Clarke's column neurons, do not possess axon collaterals in the cat (Edgley and Gallimore, 1988; Houchin et al., 1983), whereas VSCTs possess spinal axon collaterals both in cats (Bras et al., 1988) and in mice (this study). If DSCTs indeed lack spinal axon collaterals as is the case in cat, it is conceivable that DSCTs do not have access to spinal locomotor circuits and therefore might not be involved in locomotor rhythmogenesis. To further dissect the direct role of these two SCTs, future experiments are needed in which yet-to-be identified genetic markers that selectively label DSCTs and VSCTs could be used to either activate or silence them selectively using Cre-Lox recombination and floxed chemogenetic approaches.

STAR★METHODS

Detailed methods are provided in the online version of this paper and include the following:

SUPPLEMENTAL INFORMATION

Supplemental information can be found online at https://doi.org/10.1016/j.cell.2021.12.014.

ACKNOWLEDGMENTS

We thank D. Ginty for the Cdx2^{FlpO} mice and T. Jessell for the Chx10^{Cre} mice. We are also grateful to L. Pellizzoni, S. Przedborski, F.J. Alvarez, J. Gogos, M.J. O'Donovan, and members of the Mentis lab for comments on the manuscript. G.Z.M. is supported by NINDS, NIH (R01-NS078375, R21-NS079981), the NIH Blueprint for Neuroscience Research (R01-AA027079), the SMA Foundation, and Project-ALS. J.I.C. was supported by NINDS, NIH (F30NS098551).

AUTHOR CONTRIBUTIONS

G.Z.M. conceived the project. J.I.C. and G.Z.M. designed the experiments. J.I.C., M.L.M.S., and J.G.P. conducted the experiments and analyzed data. A.J.M. produced the rabies viruses and assisted with analysis and interpretation of results. G.Z.M. contributed in some experiments and analysis. J.I.C. and G.Z.M. wrote the manuscript with input from all authors.

DECLARATION OF INTERESTS

The authors declare no competing interests.

INCLUSION AND DIVERSITY

One or more of the authors of this paper self-identifies as an underrepresented ethnic minority in science.

Received: January 26, 2021
Revised: November 9, 2021
Accepted: December 13, 2021
Published: January 20, 2022

REFERENCES

Abraira, V.E., Kuehn, E.D., Chirila, A.M., Springel, M.W., Toliver, A.A., Zimmerman, A.L., Orefice, L.L., Boyle, K.A., Bai, L., Song, B.J., et al. (2017). The cellular and synaptic architecture of the mechanosensory dorsal horn. Cell *168*, 295–310.e19.

Al-Mosawie, A., Wilson, J.M., and Brownstone, R.M. (2007). Heterogeneity of V2-derived interneurons in the adult mouse spinal cord. Eur. J. Neurosci. *26*, 3003–3015.

Alvarez, F.J., and Fyffe, R.E. (2007). The continuing case for the Renshaw cell. J. Physiol. *584*, 31–45.

Arshavsky, Y.I., Berkinblit, M.B., Fukson, O.I., Gelfand, I.M., and Orlovsky, G.N. (1972). Origin of modulation in neurones of the ventral spinocerebellar tract during locomotion. Brain Res *43*, 276–279.

Atkinson, L., Batten, T.F., Moores, T.S., Varoqui, H., Erickson, J.D., and Deuchars, J. (2004). Differential co-localisation of the P2X7 receptor subunit with vesicular glutamate transporters VGLUT1 and VGLUT2 in rat CNS. Neuroscience *123*, 761–768.

Baldissera, F., and Roberts, W.J. (1975). Effects on the ventral spinocerebellar tract neurones from Deiters' nucleus and the medial longitudinal fascicle in the cat. Acta Physiol. Scand. *93*, 228–249.

Bentivoglio, M., and Kuypers, H.G. (1982). Divergent axon collaterals from rat cerebellar nuclei to diencephalon, mesencephalon, medulla oblongata and cervical cord. A fluorescent double retrograde labeling study. Exp. Brain Res. *46*, 339–356.

Bikoff, J.B., Gabitto, M.I., Rivard, A.F., Drobac, E., Machado, T.A., Miri, A., Brenner-Morton, S., Famojure, E., Diaz, C., Alvarez, F.J., Mentis, G.Z., and Jessell, T.M. (2016). Spinal Inhibitory Interneuron Diversity Delineates Variant Motor Microcircuits. Cell *165*, 207–219.

Bonnot, A., Mentis, G.Z., Skoch, J., and O'Donovan, M.J. (2005). Electroporation loading of calcium-sensitive dyes into the CNS. J. Neurophysiol. *93*, 1793–1808.

Bonnot, A., Whelan, P.J., Mentis, G.Z., and O'Donovan, M.J. (2002). Locomotor-like activity generated by the neonatal mouse spinal cord. Brain Res. Brain Res. Rev. *40*, 141–151.

Bouvier, J., Caggiano, V., Leiras, R., Caldeira, V., Bellardita, C., Balueva, K., Fuchs, A., and Kiehn, O. (2015). Descending command neurons in the brainstem that halt locomotion. Cell *163*, 1191–1203.

Bras, H., Cavallari, P., and Jankowska, E. (1988). Demonstration of initial axon collaterals of cells of origin of the ventral spinocerebellar tract in the cat. J. Comp. Neurol. *273*, 584–592.

Britz, O., Zhang, J., Grossmann, K.S., Dyck, J., Kim, J.C., Dymecki, S., Gosgnach, S., and Goulding, M. (2015). A genetically defined asymmetry underlies the inhibitory control of flexor-extensor locomotor movements. eLife *4*, e04718.

Cazalets, J.R., Borde, M., and Clarac, F. (1995). Localization and organization of the central pattern generator for hindlimb locomotion in newborn rat. J. Neurosci. *15*, 4943–4951.

Chang, Q., Gonzalez, M., Pinter, M.J., and Balice-Gordon, R.J. (1999). Gap junctional coupling and patterns of connexin expression among neonatal rat lumbar spinal motor neurons. J. Neurosci. *19*, 10813–10828.

Chen, A.I., de Nooij, J.C., and Jessell, T.M. (2006). Graded activity of transcription factor Runx3 specifies the laminar termination pattern of sensory axons in the developing spinal cord. Neuron *49*, 395–408.

Chopek, J.W., Nascimento, F., Beato, M., Brownstone, R.M., and Zhang, Y. (2018). Sub-populations of spinal V3 interneurons form focal modules of layered pre-motor microcircuits. Cell Rep *25*, 146–156.e3.

Cooper, S., and Sherrington, C.S. (1940). Gowers tract and spinal border cells. Brain *63*, 123–134.

Crone, S.A., Quinlan, K.A., Zagoraiou, L., Droho, S., Restrepo, C.E., Lundfald, L., Endo, T., Setlak, J., Jessell, T.M., Kiehn, O., et al. (2008). Genetic ablation of V2a ipsilateral interneurons disrupts left-right locomotor coordination in mammalian spinal cord. Neuron *60*, 70–83.

Crone, S.A., Zhong, G., Harris-Warrick, R., and Sharma, K. (2009). In mice lacking V2a interneurons, gait depends on speed of locomotion. J. Neurosci. *29*, 7098–7109.

Earhart, G.M., and Bastian, A.J. (2001). Selection and coordination of human locomotor forms following cerebellar damage. J. Neurophysiol. *85*, 759–769.

Eccles, J.C., Fatt, P., and Koketsu, K. (1954). Cholinergic and inhibitory synapses in a pathway from motor-axon collaterals to motoneurones. J. Physiol. *126*, 524–562.

Edgley, S.A., and Gallimore, C.M. (1988). The morphology and projections of dorsal horn spinocerebellar tract neurones in the cat. J. Physiol. *397*, 99–111.

Enjin, A., Perry, S., Hilscher, M.M., Nagaraja, C., Larhammar, M., Gezelius, H., Eriksson, A., Leão, K.E., and Kullander, K. (2017). Developmental disruption of recurrent inhibitory feedback results in compensatory adaptation in the Renshaw cell-motor neuron circuit. J. Neurosci. *37*, 5634–5647.

Falgairolle, M., Puhl, J.G., Pujala, A., Liu, W., and O'Donovan, M.J. (2017). Motoneurons regulate the central pattern generator during drug-induced locomotor-like activity in the neonatal mouse. eLife *6*, e26622.

Federico, F., Leggio, M.G., Mandolesi, L., and Petrosini, L. (2006). The NMDA receptor antagonist CGS 19755 disrupts recovery following cerebellar lesions. Restor. Neurol. Neurosci. *24*, 1–7.

Fletcher, E.V., Simon, C.M., Pagiazitis, J.G., Chalif, J.I., Vukojicic, A., Drobac, E., Wang, X., and Mentis, G.Z. (2017). Reduced sensory synaptic excitation impairs motor neuron function via Kv2.1 in spinal muscular atrophy. Nat. Neurosci. *20*, 905–916.

Garcia-Rill, E. (1986). The basal ganglia and the locomotor regions. Brain Res *396*, 47–63.

Gosgnach, S., Bikoff, J.B., Dougherty, K.J., El Manira, A., Lanuza, G.M., and Zhang, Y. (2017). Delineating the diversity of spinal interneurons in locomotor circuits. J. Neurosci. *37*, 10835–10841.

Gosgnach, S., Lanuza, G.M., Butt, S.J., Saueressig, H., Zhang, Y., Velasquez, T., Riethmacher, D., Callaway, E.M., Kiehn, O., and Goulding, M. (2006). V1 spinal neurons regulate the speed of vertebrate locomotor outputs. Nature *440*, 215–219.

Goulding, M., and Pfaff, S.L. (2005). Development of circuits that generate simple rhythmic behaviors in vertebrates. Curr. Opin. Neurobiol. *15*, 14–20.

Graham Brown, T. (1911). The intrinsic factors in the act of progression in the mammal. Proc. R. Soc. Lond. B. *84*, 308–319.

Grillner, S. (2003). The motor infrastructure: from ion channels to neuronal networks. Nat. Rev. Neurosci. *4*, 573–586.

Grillner, S., and Wallén, P. (1985). Central pattern generators for locomotion, with special reference to vertebrates. Annu. Rev. Neurosci. *8*, 233–261.

Guertin, P.A. (2012). Central pattern generator for locomotion: anatomical, physiological, and pathophysiological considerations. Front. Neurol. *3*, 183.

Hägglund, M., Borgius, L., Dougherty, K.J., and Kiehn, O. (2010). Activation of groups of excitatory neurons in the mammalian spinal cord or hindbrain evokes locomotion. Nat. Neurosci. *13*, 246–252.

Hammar, I., Krutki, P., Drzymala-Celichowska, H., Nilsson, E., and Jankowska, E. (2011). A trans-spinal loop between neurones in the reticular formation and in the cerebellum. J. Physiol. *589*, 653–665.

Houchin, J., Maxwell, D.J., Fyffe, R.E., and Brown, A.G. (1983). Light and electron microscopy of dorsal spinocerebellar tract neurones in the cat: an intracellular horseradish peroxidase study. Q. J. Exp. Physiol. *68*, 719–732.

Ilg, W., Giese, M.A., Gizewski, E.R., Schoch, B., and Timmann, D. (2008). The influence of focal cerebellar lesions on the control and adaptation of gait. Brain *131*, 2913–2927.

Jankowska, E., Nilsson, E., and Hammar, I. (2011). Processing information related to centrally initiated locomotor and voluntary movements by feline spinocerebellar neurones. J. Physiol. *589*, 5709–5725.

Jiang, Z., Carlin, K.P., and Brownstone, R.M. (1999). An *in vitro* functionally mature mouse spinal cord preparation for the study of spinal motor networks. Brain Res *816*, 493–499.

Jordan, L.M., Liu, J., Hedlund, P.B., Akay, T., and Pearson, K.G. (2008). Descending command systems for the initiation of locomotion in mammals. Brain Res. Rev. *57*, 183–191.

Kase, D., and Imoto, K. (2012). The role of HCN channels on membrane excitability in the nervous system. J. Signal Transduct. *2012*, 619747.

Kiehn, O. (2006). Locomotor circuits in the mammalian spinal cord. Annu. Rev. Neurosci. *29*, 279–306.

Kiehn, O. (2016). Decoding the organization of spinal circuits that control locomotion. Nat. Rev. Neurosci. *17*, 224–238.

Kiehn, O., and Butt, S.J. (2003). Physiological, anatomical and genetic identification of CPG neurons in the developing mammalian spinal cord. Prog. Neurobiol. *70*, 347–361.

Kjaerulff, O., and Kiehn, O. (1996). Distribution of networks generating and coordinating locomotor activity in the neonatal rat spinal cord *in vitro*: a lesion study. J. Neurosci. *16*, 5777–5794.

Lev-Tov, A., Delvolvé, I., and Kremer, E. (2000). Sacrocaudal afferents induce rhythmic efferent bursting in isolated spinal cords of neonatal rats. J. Neurophysiol. *83*, 888–894.

Lundberg, A. (1971). Function of the ventral spinocerebellar tract. A new hypothesis. Exp. Brain Res. *12*, 317–330.

Lüthi, A., and McCormick, D.A. (1998). H-current: properties of a neuronal and network pacemaker. Neuron *21*, 9–12.

Manvich, D.F., Webster, K.A., Foster, S.L., Farrell, M.S., Ritchie, J.C., Porter, J.H., and Weinshenker, D. (2018). The DREADD agonist clozapine N-oxide (CNO) is reverse-metabolized to clozapine and produces clozapine-like interoceptive stimulus effects in rats and mice. Sci. Rep. *8*, 3840.

Martínez-Silva, L., Manjarrez, E., Gutiérrez-Ospina, G., and Quevedo, J.N. (2014). Electrophysiological representation of scratching CpG activity in the cerebellum. PLoS One *9*, e109936.

Matsushita, M., and Hosoya, Y. (1978). The location of spinal projection neurons in the cerebellar nuclei (cerebellospinal tract neurons) of the cat. A study with the horseradish peroxidase technique. Brain Res *142*, 237–248.

Meehan, C.F., Grondahl, L., Nielsen, J.B., and Hultborn, H. (2012). Fictive locomotion in the adult decerebrate and spinal mouse *in vivo*. J. Physiol. *590*, 289–300.

Meehan, C.F., Mayr, K.A., Manuel, M., Nakanishi, S.T., and Whelan, P.J. (2017). Decerebrate mouse model for studies of the spinal cord circuits. Nat. Protoc. *12*, 732–747.

Mendelsohn, A.I., Simon, C.M., Abbott, L.F., Mentis, G.Z., and Jessell, T.M. (2015). Activity regulates the incidence of heteronymous sensory-motor connections. Neuron *87*, 111–123.

Mentis, G.Z., Alvarez, F.J., Bonnot, A., Richards, D.S., Gonzalez-Forero, D., Zerda, R., and O'Donovan, M.J. (2005). Noncholinergic excitatory actions of motoneurons in the neonatal mammalian spinal cord. Proc. Natl. Acad. Sci. USA *102*, 7344–7349.

Mentis, G.Z., Blivis, D., Liu, W., Drobac, E., Crowder, M.E., Kong, L., Alvarez, F.J., Sumner, C.J., and O'Donovan, M.J. (2011). Early functional impairment of sensory-motor connectivity in a mouse model of spinal muscular atrophy. Neuron *69*, 453–467.

Mentis, G.Z., Díaz, E., Moran, L.B., and Navarrete, R. (2002). Increased incidence of gap junctional coupling between spinal motoneurones following transient blockade of NMDA receptors in neonatal rats. J. Physiol. *544*, 757–764.

Mentis, G.Z., Siembab, V.C., Zerda, R., O'Donovan, M.J., and Alvarez, F.J. (2006). Primary afferent synapses on developing and adult Renshaw cells. J. Neurosci. *26*, 13297–13310.

Morton, S.M., and Bastian, A.J. (2003). Relative contributions of balance and voluntary leg-coordination deficits to cerebellar gait ataxia. J. Neurophysiol. *89*, 1844–1856.

Nishimaru, H., Restrepo, C.E., Ryge, J., Yanagawa, Y., and Kiehn, O. (2005). Mammalian motor neurons corelease glutamate and acetylcholine at central synapses. Proc. Natl. Acad. Sci. USA *102*, 5245–5249.

Noga, B.R., Shefchyk, S.J., Jamal, J., and Jordan, L.M. (1987). The role of Renshaw cells in locomotion: antagonism of their excitation from motor axon collaterals with intravenous mecamylamine. Exp. Brain Res. *66*, 99–105.

O'Donovan, M.J., Bonnot, A., Mentis, G.Z., Chub, N., Pujala, A., and Alvarez, F.J. (2010). Mechanisms of excitation of spinal networks by stimulation of the ventral roots. Ann. N. Y. Acad. Sci. *1198*, 63–71.

Pape, H.C. (1996). Queer current and pacemaker: the hyperpolarization-activated cation current in neurons. Annu. Rev. Physiol. *58*, 299–327.

Pastor, A.M., Mentis, G.Z., De La Cruz, R.R., Díaz, E., and Navarrete, R. (2003). Increased electrotonic coupling in spinal motoneurons after transient botulinum neurotoxin paralysis in the neonatal rat. J. Neurophysiol. *89*, 793–805.

Personius, K.E., Chang, Q., Mentis, G.Z., O'Donovan, M.J., and Balice-Gordon, R.J. (2007). Reduced gap junctional coupling leads to uncorrelated motor neuron firing and precocious neuromuscular synapse elimination. Proc. Natl. Acad. Sci. USA *104*, 11808–11813.

Picton, L.D., Sillar, K.T., and Zhang, H.Y. (2018). Control of Xenopus tadpole locomotion via selective expression of Ih in excitatory interneurons. Curr. Biol. *28*, 3911–3923.e2.

Pisotta, I., and Molinari, M. (2014). Cerebellar contribution to feedforward control of locomotion. Front. Hum. Neurosci. *8*, 475.

Rand, M.K., Wunderlich, D.A., Martin, P.E., Stelmach, G.E., and Bloedel, J.R. (1998). Adaptive changes in responses to repeated locomotor perturbations in cerebellar patients. Exp. Brain Res. *122*, 31–43.

Reardon, T.R., Murray, A.J., Turi, G.F., Wirblich, C., Croce, K.R., Schnell, M.J., Jessell, T.M., and Losonczy, A. (2016). Rabies virus CVS-N2c(ΔG) strain enhances retrograde synaptic transfer and neuronal viability. Neuron *89*, 711–724.

Renshaw, B. (1946). Central effects of centripetal impulses in axons of spinal ventral roots. J. Neurophysiol. *9*, 191–204.

Richards, D.S., Griffith, R.W., Romer, S.H., and Alvarez, F.J. (2014). Motor axon synapses on Renshaw cells contain higher levels of aspartate than glutamate. PLoS One *9*, e97240.

Roberts, B.L., van Rossem, A., and de Jager, S. (1992). The influence of cerebellar lesions on the swimming performance of the trout. J. Exp. Biol. *167*, 171–178.

Rothberg, B.S., Shin, K.S., Phale, P.S., and Yellen, G. (2002). Voltage-controlled gating at the intracellular entrance to a hyperpolarization-activated cation channel. J. Gen. Physiol. *119*, 83–91.

Sathyamurthy, A., Barik, A., Dobrott, C.I., Matson, K.J.E., Stoica, S., Pursley, R., Chesler, A.T., and Levine, A.J. (2020). Cerebellospinal neurons regulate motor performance and motor learning. Cell Rep *31*, 107595.

Schneider, C.A., Rasband, W.S., and Eliceiri, K.W. (2012). NIH Image to ImageJ: 25 years of image analysis. Nature Methods *9*, 671–675.

Shakya Shrestha, S., Bannatyne, B.A., Jankowska, E., Hammar, I., Nilsson, E., and Maxwell, D.J. (2012). Inhibitory inputs to four types of spinocerebellar tract neurons in the cat spinal cord. Neuroscience *226*, 253–269.

Shrestha, S.S., Bannatyne, B.A., Jankowska, E., Hammar, I., Nilsson, E., and Maxwell, D.J. (2012). Excitatory inputs to four types of spinocerebellar tract neurons in the cat and the rat thoraco-lumbar spinal cord. J. Physiol. *590*, 1737–1755.

Simon, C.M., Dai, Y., Van Alstyne, M., Koutsioumpa, C., Pagiazitis, J.G., Chalif, J.I., Wang, X., Rabinowitz, J.E., Henderson, C.E., Pellizzoni, L., et al. (2017). Converging mechanisms of p53 activation drive motor neuron degeneration in spinal muscular atrophy. Cell Rep *21*, 3767–3780.

Smith, J.C., and Feldman, J.L. (1987). *In vitro* brainstem-spinal cord preparations for study of motor systems for mammalian respiration and locomotion. J. Neurosci. Methods *21*, 321–333.

Song, J., Ampatzis, K., Björnfors, E.R., and El Manira, A. (2016). Motor neurons control locomotor circuit function retrogradely via gap junctions. Nature *529*, 399–402.

Talpalar, A.E., Bouvier, J., Borgius, L., Fortin, G., Pierani, A., and Kiehn, O. (2013). Dual-mode operation of neuronal networks involved in left-right alternation. Nature *500*, 85–88.

Thoby-Brisson, M., Telgkamp, P., and Ramirez, J.M. (2000). The role of the hyperpolarization-activated current in modulating rhythmic activity in the isolated respiratory network of mice. J. Neurosci. *20*, 2994–3005.

Tresch, M.C., and Kiehn, O. (2000). Motor coordination without action potentials in the mammalian spinal cord. Nat. Neurosci. *3*, 593–599.

Udo, M., Matsukawa, K., Kamei, H., and Oda, Y. (1980). Cerebellar control of locomotion: effects of cooling cerebellar intermediate cortex in high decerebrate and awake walking cats. J. Neurophysiol. *44*, 119–134.

Walton, K.D., and Navarrete, R. (1991). Postnatal changes in motoneurone electrotonic coupling studied in the *in vitro* rat lumbar spinal cord. J. Physiol. *433*, 283–305.

Whelan, P., Bonnot, A., and O'Donovan, M.J. (2000). Properties of rhythmic activity generated by the isolated spinal cord of the neonatal mouse. J. Neurophysiol. *84*, 2821–2833.

Wirth, F.P., and O'Leary, J.L. (1974). Locomotor behavior of decerebellated arboreal mammals–monkey and raccoon. J. Comp. Neurol. *157*, 53–85.

Yu, F., Jiang, Q.J., Sun, X.Y., and Zhang, R.W. (2015). A new case of complete primary cerebellar agenesis: clinical and imaging findings in a living patient. Brain *138*, e353.

Zhang, J., Lanuza, G.M., Britz, O., Wang, Z., Siembab, V.C., Zhang, Y., Velasquez, T., Alvarez, F.J., Frank, E., and Goulding, M. (2014). V1 and v2b interneurons secure the alternating flexor-extensor motor activity mice require for limbed locomotion. Neuron *82*, 138–150.

Zhang, Y., Narayan, S., Geiman, E., Lanuza, G.M., Velasquez, T., Shanks, B., Akay, T., Dyck, J., Pearson, K., Gosgnach, S., et al. (2008). V3 spinal neurons establish a robust and balanced locomotor rhythm during walking. Neuron *60*, 84–96.

Zhang, Y., Oliva, R., Gisselmann, G., Hatt, H., Guckenheimer, J., and Harris-Warrick, R.M. (2003). Overexpression of a hyperpolarization-activated cation current (Ih) channel gene modifies the firing activity of identified motor neurons in a small neural network. J. Neurosci. *23*, 9059–9067.

Ziskind-Conhaim, L., and Hochman, S. (2017). Diversity of molecularly defined spinal interneurons engaged in mammalian locomotor pattern generation. J. Neurophysiol. *118*, 2956–2974.

Ziskind-Conhaim, L., Mentis, G.Z., Wiesner, E.P., and Titus, D.J. (2010). Synaptic integration of rhythmogenic neurons in the locomotor circuitry: the case of Hb9 interneurons. Ann. N. Y. Acad. Sci. *1198*, 72–84.

STAR★METHODS

KEY RESOURCES TABLE

REAGENT or RESOURCE	SOURCE	IDENTIFIER
Antibodies		
Chicken polyclonal Anti-green fluorescent protein	Aves Labs	Cat# GFP-1010; RRID: AB_10000240
Chicken polyclonal Anti-parvalbumin	Covance	Customized
Guinea Pig polyclonal Anti-vesicular acetylcholine transporter	Covance	Customized
Guinea Pig polyclonal Anti-synaptophysin	Synaptic Systems	Cat# 101 004; RRID:AB_1210382
Guinea Pig polyclonal Anti-vesicular glutamate transporter 1	Covance	Customized
Guinea Pig polyclonal Anti-vesicular glutamate transporter 2	Millipore Sigma	Cat# AB2251; RRID:AB_2665454
Mouse monoclonal Anti-HA	Abcam	Cat# ab130275; RRID:AB_11156884
Mouse monoclonal Anti-NEUronal Nuclei; clone A60	Millipore Sigma	Cat# MAB377; RRID:AB_2298772
Rabbit polyclonal Anti-ankyrin G	Santa Cruz	Cat# sc-28561; RRID:AB_633909
Rabbit polyclonal Anti-choline acetyltransferase	Millipore Sigma	Cat# AB144P; RRID:AB_2079751
Rabbit polyclonal Anti-DsRed	Takara	Cat# 632496; RRID:AB_10013483
Rabbit polyclonal Anti-green fluorescent protein	Novus Biologicals	Cat# NB600-308; RRID:AB_10003058
Rabbit polyclonal Anti-HA	Abcam	Cat# ab9110; RRID:AB_307019
Rabbit monoclonal Anti-HA	Abcam	Cat# ab236632; RRID:AB_2864361
Streptavidin−Cy3™ from Streptomyces avidin	Sigma-Aldrich	S6402
Anti-Digoxigenin-AP	Roche	11093274910; RRID:AB_514497
Bacterial and virus strains		
AAV2/1-Flex-nGFP-N2c-Gp-TVA	Andrew Murray Lab (Reardon et al., 2016)	N/A
AAV9-ChB-DiO-eGFP	Vector Biolabs	N/A
CAV2-CMV-GFP	Plateforme de Vectorologie de Montpellier	N/A
CAV2-CMV-Cre	Plateforme de Vectorologie de Montpellier	N/A
CAV2-CMV-Cre-GFP	Plateforme de Vectorologie de Montpellier	N/A
Rabies-N2c-hChR2-YFP	Andrew Murray Lab (Reardon et al., 2016)	Produced from Addgene plasmid #73465
Rabies-N2c-EnvA-DsRed	Andrew Murray Lab (Reardon et al., 2016)	Produced from Addgene plasmid #73460
pCRII-Topo Vglut2 in situ probe	Jeffrey Macklis Lab; Addgene	CAT#; RRID 45639
Chemicals, peptides, and recombinant proteins		
Alexa Fluor 488 Hydrazide	Invitrogen	CAT# A10436
Alexa Fluor 555 Hydrazide	Invitrogen	CAT# A20501MP
all trans-Retinal	Sigma-Aldrich	CAS# 116-31-4
Calcium sensitive dye calcium green-1 hexapotassium salt	Thermofisher/ Invitrogen	CAT# O6806
Carbenoxolone disodium	Tocris	CAT# 3096
Cascade Blue Dextran	Invitrogen	CAT# D1976
Cholera Toxin Subunit B (Recombinant), Alexa Fluor 555 Conjugate	Invitrogen	CAT# C22843
Cholera Toxin Subunit B (Recombinant), Alexa Fluor 488 Conjugate	Invitrogen	CAT# C22841
Cholera Toxin Subunit B (Recombinant), Alexa Fluor 647 Conjugate	Invitrogen	CAT# C34778
Clozapine N-oxide	Invitrogen	CAT# 4936
Dopamine hydrochloride	Tocris	CAT# 3548
Fluorescein Dextran	Invitrogen	CAT# D1821

(*Continued on next page*)

Continued

REAGENT or RESOURCE	SOURCE	IDENTIFIER
Mecamylamine hydrochloride	Tocris	CAT# 2843
NBQX disodium salt	Tocris	CAT# 1044
NEUROBIOTIN	Vector Laboratories	REF# SP-1120
NMDA	Tocris	CAT# 0114
Serotonin hydrochloride	Tocris	CAT# 3547
Texas Red Dextran	Invitrogen	CAT# D1828
ZD 7288	Tocris	CAT# 1000
Critical commercial assays		
HNPP Fluorescent Detection Set	Roche	CAT# 11758888001
Experimental models: Organisms/strains		
Mouse: C57BL/6J	JAX	#000664; RRID:IMSR_JAX:000664
Mouse: B6.Cg-Gt(ROSA)26Sortm32(CAG-COP4*H134R/EYFP)Hze/J	JAX	#024109; RRID:IMSR_JAX:024109
Mouse: B6.129-Gt(ROSA)26Sortm1(CAG-CHRM4*,-mCitrine)Ute/J	JAX	#026219; RRID:IMSR_JAX:026219
Mouse: B6.Cg-Gt(ROSA)26Sortm40.1(CAG-aop3/EGFP)Hze/J	JAX	#021188; RRID:IMSR_JAX:021188
Mouse: B6;129S6-Gt(ROSA)26Sortm9(CAG-mCherry,-CHRM4*)Dym/J	JAX	#029040; RRID:IMSR_JAX:029040
Mouse: FVB/N-Tg(Cdx2-flpo)2Ddg/J	JAX	#030288; RRID:IMSR_JAX:030288
Mouse: Chx10-CRE	Thomas Jessell Lab (Crone et al., 2008)	N/A
Oligonucleotides		
Primers for B6.Cg-Gt(ROSA)26Sortm32(CAG-COP4*H134R/EYFP)Hze/J. Wild type Forward: AAGGGAGCTGCAGTGGAGTA. Wild type Reverse: CCGAAAAT CTGTGGGAAGTC. Mutant Forward: ACATGGTCCTGCTGGAGTTC. Mutant Reverse: GGCATTAAAGCAGCGTATCC	Millipore Sigma/The Jackson Laboratory	N/A
Primers for B6.129-Gt(ROSA)26Sortm1(CAG-CHRM4*, -mCitrine)Ute/J. Wild type Forward: CGTGATCTGCAACTCCAGTC. Wild type Reverse: CCGAAAATC TGTGGGAAGTC. Mutant Forward: TGA. Mutant Reverse: GACTGATTGCCCGAGCTG	Millipore Sigma/The Jackson Laboratory	N/A
Software and algorithms		
Clampex v10.2	Molecular Devices	https://www.moleculardevices.com
GraphPad Prism 6	GraphPad Prism	https://www.graphpad.com/
ImageJ software	Schneider et al., 2012	https://imagej.github.io/
LASAF software	Leica	https://www.leica-microsystems.com
Neurolucida	MBF Bioscience	https://www.mbfbioscience.com
OBS Studio 27.0.1 software	Open Broadcaster Software	https://obsproject.com
Oriana v4.02	Kovach Computing Service	https://www.kovcomp.co.uk
SOF-812 Activity Monitor software	Med Associates	https://www.med-associates.com
Video software VLC 3.016 Vetinari	VideoLAN	https://www.videolan.org
Other		
2-photon laser	MaiTai DeepSee, Spectral Physics	N/A
A365, current stimulus isolator	WPI, Sarasota, FL	N/A
Borosilicate glass capillary with filament	Sutter Instruments	N/A
Digidata 1440A	Molecular Devices	N/A
ECM 830 electroporation system	BTX	N/A
Multiclamp 700B	Molecular Devices	N/A
P-1000 puller	Sutter Instruments	N/A
SP5 or SP8 Leica confocal microscope	Leica	N/A
Video camera USB3.0, 2.8mm IR1/2.5” 3MP C lens	Marshall	N/A

RESOURCE AVAILABILITY

Lead contact

Further information and requests for resources and reagents should be directed to and will be fulfilled by the lead contact, George Z. Mentis (gzmentis@columbia.edu).

Materials availability

No new mouse lined were generated in this study. Requests for information for mouse lines used in this study should be directed to and will be fulfilled by George Z. Mentis (gzmentis@columbia.edu).

Data and code availability

- All data reported in this paper will be shared by the lead contact upon request.
- This paper does not report original code.
- Any additional information required to reanalyze the data reported in this paper is available from the lead contact upon request.

EXPERIMENTAL MODEL AND SUBJECT DETAILS

Mice

All surgical procedures were performed on postnatal mice in accordance with the National Institutes of Health Guidelines on the Care and Use of Animals and approved by the Columbia Animal Care and Use Committee (IACUC). Animals of both sexes were used in this study.

The original breeder pairs of C57BL6 mice (Jax Stock #000664), *lsl*-Channelrhodopsin2 mice (Ai32; Jax Stock #024109), *lsl*-hM4Di (inhibitory DREADDs) mice (Jax Stock #026219), *lsl*-Archaerhodopsin-3 mice (Ai40D; Jax Stock #021188), and *fsf-lsl*-hM4Di (inhibitory DREADDs) mice (Jax Stock #029040) used in this study were obtained from Jackson Laboratories. The Cdx2-NSE-FlpO mice (Jax Stock #030288) were a kind gift by Dr. David Ginty (Harvard University). The Chx10-CRE mice were a kind gift by Dr. Tom Jessell (Columbia University).

METHOD DETAILS

Genotyping

Genotyping protocols were carried out using standard procedures as described in detail on the Jackson website (www.jax.org). In brief, at P0 (postnatal day 0) tail DNA was extracted from mice and lysed using lysis buffer (100mM Tris pH 8, 5mM EDTA, 0.2% SDS, 200mM NaCl, 100 μg/ml Proteinase K) for 45 minutes at 55°C. PCR primers used to genotype are described on the Jackson website (www.jax.org). A universal PCR reaction consisted of: 12.5 μl of GoTaq Hot Start Green Master Mix (Promega), 0.5 μl of each primer (25 μM; Sigma), and 4 μl of 1:20 diluted lysed tail DNA into a final volume of 25 μl using ddH_2O. For the *lsl*-Channelrhodopsin2 mice, the *lsl*-Archaerhodopsin-3 mice, the *lsl*-hM4Di mice, and the *fsf-lsl*-hM4Di mice the following PCR parameters were used: 95°C for 2 mins, followed by 35 cycles of [95°C for 40 secs, 59°C for 30 secs, 72°C for 1 min], and 72°C for 5 mins. Additional information for oligonucleotides are shown in Table S1.

Immunohistochemistry and confocal analysis

Many of the immunohistochemistry protocols have been previously described (Fletcher et al., 2017; Mentis et al., 2011). In brief, animals were transcardially perfused with 4% PFA, spinal cords dissected and post-fixed in 4% paraformaldehyde (PFA) at 4°C overnight. Transverse 75μm sections were cut on a vibratome after embedding in warm 5% Agar. After blocking in 10% normal donkey serum in 0.01M PBS with 0.3% Triton X-100 (PBS-T; pH 7.4), sections were incubated overnight at room temperature with primary antibodies in the blocking solution. Primary antibodies used in this study included: ChAT, Goat, 1:100 (Millipore); VAChT, Guinea pig, 1:2000 (custom); GFP, Chicken, 1:1000 (Aves Labs, Inc.); GFP, Rabbit, 1:100 (Novus); DsRed, Rabbit, 1:100 (Takara); HA, Rabbit, 1:100 (Abcam); NeuN, Mouse, 1:500 (Millipore); Synaptophysin, Guinea pig, 1:1000 (Synaptic Systems); Parvalbumin, Chicken, 1:20000 (custom); VGluT1, Guinea pig, 1:5000 (custom); VGluT2, Guinea Pig, 1:500 (Millipore); AnkG, 1:500, Rabbit (Santa Cruz). To reveal neurons that were recorded from intracellularly and filled with Neurobiotin, spinal cords were immersion fixed in 4% PFA overnight. Subsequently, streptavidin-Cy3 (Sigma) was used at a dilution of 1:100. Streptavidin was applied to the spinal cord sections and incubated overnight at room temperature along with any primary antibodies in the blocking solution. The following day, sections were washed in PBS-T and incubated with the appropriate species-specific secondary antibody (Jackson ImmunoResearch Laboratories, Inc.) diluted at 1:250 in PBS-T for 3 hours at room temperature. Sections were washed with PBS and mounted on glass slides with 70% glycerol / 30% PBS.

Sections were imaged using either a SP5 or SP8 Leica confocal microscope. Images were scanned with either a 20x air objective, 40x oil objective, or 63x oil objective. All images were analyzed in either LASAF software (Leica) or ImageJ software. For VSCT neuron transduction counts, we analyzed z-stack images (at 3 μm intervals) of each section. VSCT neuronal counts were performed with

confocal microscopy in 75μm thick sections. We established that the L1 spinal segment in P45 mice extends in the rostro-caudal axis over 17 transverse sections (75 μm thickness). The number of VSCT was determined by counting all neurons ventral to the medio-lateral line emanating from the central canal, through z-stack scanning at 0.5 μm z-axis intervals. This was repeated in three L1 spinal cord transverse sections. The average number of VSCT from these sections was multiplied by 17 (the total number of sections within the L1 spinal segment). The number of VSCT neurons was calculated from the projection image obtained by all z-stack optical sections for every one of the 3 randomly chosen L1 transverse spinal cord sections. The same method was also applied for DSCTs and VSCTs for neuronal counts at P4-P5. At P4-P5, the number of sections in the L1 segment was 11. To determine the number of DSCTs and VSCTs at P4-P5, the number of VSCTs and DSCTs was calculated from the projection image obtained by all z-stack optical sections for every one of three randomly chosen L1 transverse spinal cord sections and multiplied by 11 (the total number of sections within the L1 spinal segment at P4-P5). DSCTs were defined as the all neurons positioned dorsal to the medio-lateral line emanating from the central canal.

For dye coupling confocal microscopy analysis, a single VSCT neuron was recorded, filled and analyzed per each mouse (n=12 VSCTs from N=12 mice).

Orthograde and retrograde fills using the *ex vivo* spinal cord preparation

In some experiments, motor neurons and sensory fibers entering the spinal cord were labelled by orthograde and anterograde fills using the *ex vivo* spinal cord. Details have been previously reported (Mentis et al., 2005, 2011). Briefly, the spinal cord was dissected free under in vitro conditions at ~10°C and continuously superfused with artificial CSF (aCSF). The appropriate ventral and dorsal roots were positioned in suction electrodes and backfilled with either: i) Texas Red Dextran, ii) Cascade Blue Dextran or iii) Fluorescein Dextran [10,000 molecular weight (MW)] for ~24 h (at 10°C) to label motor neurons (from a ventral root) or sensory fibers (from a dorsal root). Following this period, the appropriate lumbar segments immersion-fixed in 4% paraformaldehyde for 24 h. The spinal cord was embedded in 5% warm agar and subsequently sectioned (75μm) using a Vibratome. The sections were collected in wells and processed further for immunohistochemistry against different antibodies by free-floating method (in wells). Finally, sections were mounted on glass slides and coverslipped using an antifading agent (PBS/glycerol, 7:3) until examination with confocal microscopy.

Fluorescence *in situ* hybridization (FISH)

Fluorescent *in situ* hybridization protocols were carried out as recently reported (Simon et al., 2017). Fresh spinal cord tissue (L1 and L2 segments) was cryopreserved in sterile 30% sucrose overnight and flash frozen in OCT on dry ice at P4. 18-20μm sections were cut on a cryostat and fixed with 4% PFA for 10 minutes. Washes were carried out as follows: 3x PBS, 1x PBS-T 10 minutes (0.1% Triton X-100), 1x PBS. Acetylation was performed for 15 minutes in 1.17% (v/v) triethanolamine and 0.25% (v/v) acetic anhydride in ddH_2O. 3x PBS washes were followed by overnight hybridization with the RNA probe at 68°C in hybridization solution (50% formamide, 5X SSC, 1X Denhart's, 1mg/ml baker's yeast RNA in ddH_2O) in a humidifying chamber. The probe was applied at 1ng/μL following denaturation through 5 minutes of warming at 85°C.

The following day, sections were washed with 0.2% SSC 2x for 15 minutes at 68°C, followed by 3x PBS washes. Blocking solution was then applied for 1 hour at room temperature (0.5% Blocking reagent [Roche] in 100 mM Tris-HCl, 150 mM NaCl; pH 7.5). Sections were then incubated with anti-digoxigenin-AP 1:500 (Roche) dissolved in blocking solution for 1 hour at 37°C. Sections were washed for 10 minutes 3x in Washing Buffer (100 mM Tris-HCl, 150 mM NaCl, 0.05% Tween 20, pH 7.5). Sections were washed for 10 minutes 2x in Detection Buffer (100 mM Tris-HCl, 100 mM NaCl, 10 mM $MgCl_2$, pH 8.0). Development was done with the HNPP Fluorescent Detection Set (Roche) as per the manufacturer's instructions for 1 hour. Sections were washed in dH_2O and mounted with 2% DABCO in 50% glycerol/PBS to preserve fluorescence.

The RNA probe for VGlut2 was obtained through a PCRII-Topo VGlut2 *in situ* probe vector from the laboratory of Dr. Jeffrey Macklis deposited in Addgene as plasmid #45639 (https://www.addgene.org). For probe generation from the linearized plasmid, RNA transcription was conducted in the presence of digoxigenin-labeled nucleotides (Roche). After transcription, probes were precipitated overnight in 410μl precipitation solution (75% EtOH, 0.25 M TE buffer, 100 mM LiCl) at -20°C. The following day, the probes were precipitated through spinning at 13,000 RPM and the supernatant decanted. The probes were washed in 1 ml of 70% ethanol, spun at 13,000 RPM, and the supernatant decanted followed by re-suspension in hybridization solution at 10 ng/μl.

CTb injections and viral gene delivery to VSCTs

VSCTs were retrogradely labeled *in vivo* by intracerebellar injection of cholera toxin B subunit (CTb) conjugated to Alexa-488, Alexa-555, or Alexa-647 (Invitrogen). Newborn P0 mice were anesthetized by isoflurane inhalation. A small incision and craniotomy over the cerebellum was made to inject ~200-600nl of 0.5-1% fluorescently-conjugated CTb in PBS using a finely-pulled glass microelectrode (P-1000 puller [Sutter Instruments]) under sterile conditions. The CTb was delivered by pressure through an adapted micro-syringe. The incision was closed with sutures. Upon dissection at P3-P5, the injection was determined to be accurate by visualization of fluorescence in the cerebellum under a fluorescence microscope (Leica) without spread to other brain tissue (Figures S1F and S1G).

For viral gene delivery, the following viruses were used: CAV2-CMV-GFP (CAV2 = Canine Adenovirus 2), titer = 1.3 x 10^{13} pp/ml [Plateforme de Vectorologie de Montpellier]); CAV2-CMV-Cre, titer = 1.4 x 10^{13} pp/ml; CAV2-CMV-Cre-GFP, titer = 1.3 x 10^{13} pp/ml; Rabies-N2c-ChR2-YFP, titer = 1x10^9 infectious particles/ml; Rabies-N2c-EnvA-DsRed, titer = ~5x10^8 infectious particles/ml, AAV2/1-Flex-nGFP-N2c-Gp-TVA; AAV9-ChB-DiO-eGFP, titer = 1.1 x 10^{11} pp/ml (Vector BioLabs). The approximate volume of virus

injected into the cerebellum was 0.5μl. WT mice of both sexes were injected intracerebellar at P0 with a 50/50 mixture of the CAV2 virus with 1% CTb-Alexa 555 or CTb-Alexa 647. At P3-P21, the spinal cord was processed for immunohistochemistry. Analysis of the extent of VSCT labeling consisted of comparing the number of VSCT neurons transduced by the virus with the number of VSCT neurons labeled by CTb using confocal images acquired with Leica confocal microscopes and analyzed with the Leica LASAF software. For the *in vivo* adult freely moving mice, mice were injected with the same viruses at P21 and examined at P35-45. For the Chx10-CRE mice experiments, AAV-Flex-nGFP-Gp-TVA was injected in the lumbar spinal cord at P0. Rabies-N2c-EnvA-DsRed was injected in the lumbar spinal cord at P10. To allow for transfection, mice were euthanized for the terminal experiments between P21-P28.

Intracellular recording

Many of the experimental protocols used in this study have been described previously (Fletcher et al., 2017; Mentis et al., 2011). At P3-P5, the animals were decapitated, the spinal cords dissected and removed under cold (~10°C) artificial cerebrospinal fluid (aCSF) containing (in mM): 128.35 NaCl, 4 KCl, 0.58 $NaH_2PO_4.H_2O$, 21 $NaHCO_3$, 30 D-Glucose, 1.5 $CaCl_2.H_2O$, and 1 $MgSO_4.7H_2O$. The spinal cord was then transferred to a customized recording chamber placed under the objective of an upright confocal microscope (Leica SP5) equipped with a 2-photon laser (MaiTai DeepSee, Spectral Physics).

The intact *ex vivo* spinal cord preparation was perfused continuously with oxygenated (95% O_2 / 5% CO_2) aCSF (~10 ml/min). The physiological solution was kept at room temperature, ranging between 21-25°C, which results in slower conduction velocity for neurons. The ventral root of the L1 or L2 and L5 spinal segments bilaterally were placed into suction electrodes for recording. All potentials were recorded in either DC or AC (0.1 Hz filter) (Cyberamp, Molecular Devices). Recordings were fed to an A/D interface (Digidata 1440A, Molecular Devices) and acquired with Clampex (v10.2, Molecular Devices) at a sampling rate of 10-20 kHz. Data were analyzed offline using Clampfit (v10.2, Molecular Devices). In some preparations, the cerebellum-brainstem-spinal cord was used, while in experiments in which locomotor-like behavior was induced either by electrical stimulation or with a cocktail of drugs, the T4-cauda equina spinal cord was used.

Whole-cell recordings were obtained with patch electrodes advanced through the lateral or ventral aspect of the spinal cord under visual guidance using 2-photon microscopy to visualize individual VSCT neurons. Patch electrodes were pulled from thin-walled borosilicate glass capillary with filament (Sutter Instruments) using a P-1000 puller (Sutter Instruments) to resistances between 5–16 MΩ. The electrodes were filled with intracellular solution containing (in mM): 10 NaCl, 130 K-Gluconate, 10 HEPES, 11 EGTA, 1 $MgCl_2$, 0.1 $CaCl_2$ and 1 Na_2ATP, 0.1 Alexa-555 or Alexa-488 hydrazide (Life Technologies), and 0.5 mg/ml Neurobiotin (Vector Labs). pH was adjusted to 7.2–7.3 with KOH. The final osmolarity of the intracellular solution was 295–305 mOsm. Bridge balance was applied to all recordings. The liquid junction potential was calculated as −2 mV but was not corrected in any of the recordings. The identity of the recorded neuron as a VSCT neuron was confirmed during the experiment by evoking an antidromic action potential by stimulation of the cerebellum through a concentric electrode applied just under the surface of the vermis of the cerebellum (0.2-0.5 ms, 1.2-3x Threshold). Threshold was determined by the minimum intensity needed to evoke a response in 3 out of 5 consecutive trials at 0.1 Hz. Upon increasing the stimulation intensity, there was no change in the amplitude of the all-or-none action potential induced. In addition, VSCT neurons were also identified by the colocalization of CTb-conjugated fluorochrome injected in the cerebellum at P0, with the intracellular fluorescent dye contained in the intracellular electrode. VSCT neurons were accepted for analysis only if the following criteria were met: (i) stable resting membrane potential of at least −45 mV (ii) an overshooting action potential and (iii) at least 20 mins of recording.

Synaptic potentials were recorded from individual VSCT neurons (DC - 3 kHz, Multiclamp 700B, Molecular Devices) in response to a brief (0.2 ms, 40-100 μA, 0.1-10 Hz) stimulation (A365, current stimulus isolator, WPI, Sarasota, FL) of the ipsilateral homosegmental ventral root (L1 or L2). Recordings contaminated by spontaneous events were discarded. The holding potential of the VSCT was varied from -80 to -40 mV to test for chemical components of synaptic responses. The jitter test was used to test whether the response was monosynaptic (Bikoff et al., 2016; Mendelsohn et al., 2015). The jitter test was conducted by analyzing the coefficient of variation at differing frequencies of ventral root stimulation (0.1, 1, 5, and 10 Hz). As previously published, if the coefficient of variation did not change over increasing stimulation frequency, the synaptic connection was determined to be monosynaptic. Conversely, if the coefficient of variation increased over increasing stimulation frequency, the synaptic connection was determined to be polysynaptic. Sequential bath application of pharmacological antagonists was used to study the components of the ventral root stimulation-mediated response in VSCTs. Drugs were allowed to perfuse into the spinal cord for at least 15 minutes or longer prior to stimulation. Mecamylamine, a nicotinic receptor antagonist, was used at a concentration of 50μM (Tocris). NBQX, an AMPA receptor antagonist, was used at a concentration of 20μM (Tocris). Carbenoxolone, a gap junction antagonist, was used at a concentration of 100μM (Tocris).

I_h current was tested by negative current injection with examination of the resulting voltage trace for the characteristic sag and post-inhibitory rebound. Sag was calculated as the absolute value of the difference between the most negative voltage reached during negative current injection and the stable plateau voltage potential. Post-inhibitory rebound was calculated as the difference between the least negative voltage reached immediately after negative current injection and the voltage prior to current injection. Time-dependency of the sag and post-inhibitory rebound was tested by injecting steps of negative current (-200 to -500 pA) over different durations (ranging from 250 ms to 5 s with steps of 250-500 ms). Traces were examined for increased sag and post-inhibitory rebound with longer negative current injections. Voltage-dependency of the sag and post-inhibitory rebound was tested by injecting a varying negative current (ranging from -50 to -600 pA with steps of 50 pA) over a set duration (1 s to 2 s). Traces were examined for

increased sag and post-inhibitory rebound with larger negative current injections which resulted in increased voltage changes in the recorded neuron. ZD7288, an HCN channel antagonist, was used at a concentration of 100 μM (Tocris).

At the end of the recording session, the electrode was removed from the spinal cord, but kept in the bath to measure any DC offset that might have occurred over the course of the recording. DC offset varied from -2 mV to +1 mV and due its low amplitude was not corrected in any of the recordings. The spinal cord was fixed in 4% PFA overnight and subsequently transferred to PBS and processed for immunohistochemistry.

Somatodendritic labeling of motor neurons

Experimental protocols used in this study have been described before (Fletcher et al., 2017; Mentis et al., 2005). After dissection and intracellular recording, the spinal cord was transferred back to the dissection chamber and the L1 or L2 ventral root was placed inside a suction electrode and backfilled with a Cascade Blue-Dextran (Invitrogen) to label the motor neurons. The spinal cord was perfused with cold (~10°C), oxygenated (95% O_2, 5% CO_2) aCSF (containing in mM: 128.35 NaCl, 4 KCl, 0.58 $NaH_2PO_4.H_2O$, 21 $NaHCO_3$, 30 D-Glucose, 0.1 $CaCl_2.H_2O$, and 2 $MgSO_4.7H_2O$). After 12 – 20 hours, the cord was immersion-fixed in 4% PFA and washed in 0.01M PBS. Sections were subsequently processed for immunohistochemistry and confocal microscopy.

Neurolucida reconstruction of VSCT neurons and Image J analysis

Spinal cord sections were cut at 75μm and processed for immunohistochemistry to enhance GFP with an anti-GFP antibody. In addition, motor neurons were labelled with ChAT immunoreactivity. In some experiments, the axon identity was verified by AnkG immunoreactivity. Single optical planes were acquired in Z-stacks at 1μm intervals for the entire thickness of the spinal cord section (~75μm). Sections were scanned using an SP5 Leica confocal microscope and analyzed using ImageJ and Neurolucida (MBF Bioscience).

For the colocalization of CTb-488, VGluT2 and synaptophysin signals (Figure S7) to mark the synapses from SCT axon collaterals, confocal images acquired with LAS (Leica) software were exported to ImageJ software as TIF format files. Then, the different channels were merged and further saved as TIF. In ImageJ software, the channels were split and the threshold adjusted. For each channel we apply the "Subtract 254" math module once. Then two channels were added together and the "threshold" was set to 2-255. This image was then converted-to-mask. For the third channel, was "made binary" and was "added" to the image processed by the addition of the first two channels.

Electroporation and 2-photon calcium imaging

The detailed experimental protocol used in this study has been described before (Bonnot et al., 2005). Briefly, at P4, the spinal cord of wild type mice was dissected and pinned down with the ventral side up, and a broken sharp glass electrode was used to pressure-apply 2μl of calcium-sensitive dye solution under the dura matter in the rostral lumbar area (L1/L2). The calcium sensitive dye calcium green-1 hexapotassium salt (1,147 MW, 55mM; Thermofisher Scientific), was dissolved in artificial cerebrospinal fluid (aCSF; as above) prior to application. Two gold-plated electrodes (BTX, 3mm in length and 0.5 mm in diameter) were submerged in the aCSF and positioned in parallel on either side of the spinal cord. Square voltage pulses (10-50 V applied voltage, 50-100 ms duration, 4-10 pulses at 1 Hz) were applied between the electrodes within 5min after dye application using the ECM 830 electroporation system (BTX). The dura mater was removed from the lateral sides to allow visualization of the labeled cells. After electroporation, the cord was left for ~1 h to allow washout of the excess of dye from the extracellular space. The spinal cord was subsequently transferred to a customized recording chamber for electrical and optical recordings (as above). The lateral side of the lumbar spinal cord was imaged continuously under two-photon microscopy, while a ventral root was stimulated. Analysis of the fluorescent signal was conducted in Leica LASAF software using the region of interest (ROI) function.

Optogenetic and chemogenetic manipulation

Optogenetic and chemogenetic manipulation experiments were carried out in either *lsl*-Channelrhodopsin2 mice, *lsl*-hM4Di mice, or *lsl*-Archaerhodopsin-3 mice, as appropriate. All mice were homozygotes for the inserted transgene. In some mice, Rabies-N2C-ChR2-YFP was also used to express ChR2 in SCT neurons following cerebellum injection. P0 mice were injected intracerebellar with the CAV2-Cre or CAV2-Cre-GFP (or CAV2-GFP as control) viral vector along with fluorescently-labeled CTb, as described above. At P3-P6, the spinal cord was dissected and the *ex vivo* neonate spinal cord preparations were transferred to the recording chamber for physiological recordings as described above. The ventral roots of the L1 and L5 spinal segments bilaterally were placed into suction electrodes, along with the L5 dorsal root and/or S3 dorsal root ganglion as described above.

For VSCT neuron activation experiments utilizing Channelrhodopsin2, 470nm light was delivered via a LED (CoolLED; pE-100) placed over the L1 and L2 segments bilaterally on the ventral surface of the spinal cord. For DSCT neuron activation, dorsal illumination was used over the L1 and L2 segments bilaterally in the same *ex vivo* spinal cord preparations used for VSCT activation, by flipping over the spinal cord and replacing the suction electrodes. LED power ranged between 53-106mW. Light was delivered with either continuous illumination for 20s or pulses of light for 100ms at 5Hz or 50ms at 10Hz for 20s. Light was delivered via a customized patch cable built by Thorlabs, Inc. Recording commenced with 1-10 seconds pre-light to establish a baseline, followed by light stimulation. Each preparation was tested for a minimum of three trials. All potentials were recorded in either DC or AC (0.1 Hz filter) (Cyberamp, Molecular Devices). For consistent Channelrhodopsin2 activation, all experiments were conducted in the presence of

1-3 μM all trans-Retinal (Sigma-Aldrich) in the aCSF. Pharmacological antagonism was used to test for the necessity of the h-current and gap junction communication in the production of locomotor-like activity following VSCT neuron photoactivation. Drugs were bath applied into the circulating aCSF and allowed to perfuse into the spinal cord for at least 15mins.

For inhibition experiments utilizing Archaerhodopsin-3, locomotor activity was induced via electrical stimulation of the S3 dorsal root ganglia. After successful induction of locomotion, 585nm light was delivered via a LED (CoolLED; pE-100) placed over the L1 and L2 segments bilaterally on the ventral surface of the spinal cord at the same time of electrically-induced locomotor-like activity. LED power was 47mW. For consistent Archaerhodopsin-3 activation, all experiments were conducted in the presence of 1-3 μM all trans-Retinal (Sigma-Aldrich) in the aCSF. Each condition was tested for a minimum of three trials. Analysis consisted of quantifying the locomotor frequency in each trace under each condition offline on Clampfit (v10.2, Molecular Devices).

For inhibition experiments utilizing inhibitory DREADDs, locomotor activity was induced via electrical stimulation of the L5 dorsal root, S3 dorsal root ganglion, or stimulation of a ventral root or through bath application of the pharmacological cocktail of drugs consisting of NMDA (5μM; Tocris), serotonin (10μM; Tocris), and dopamine (50μM; Tocris). For control experiments, CAV2-GFP was injected at P0 into the cerebellum. After successful induction of locomotion, 10μM CNO (Tocris) was bath applied in the aCSF and allowed to freely circulate for 15-30 minutes. Induced locomotor activity was then investigated assayed in the pharmacological experiments. CNO was washed out using fresh aCSF and following 30+ minutes of washout, locomotor activity was induced again under the same conditions prior to CNO exposure. Each condition (pre-drug, CNO, washout) was tested for a minimum of three trials. Analysis consisted of quantifying the locomotor frequency in each trace under each condition offline on Clampfit (v10.2, Molecular Devices).

In vivo behavioral experiments

In vivo behavioral experiments were carried out by crossing Cdx2-NSE-FlpO mice (Britz et al., 2015) with *fsf-lsl*-hM4Di (inhibitory DREADDs) mice. The resulting double transgenic pups were heterozygotes for both inserted transgenes. P21 mice were injected intracerebellar with either CAV2-GFP-CRE viral vector, or CAV2-GFP, or CTb-647, as described above. Control mice consisted of mice injected with CAV2-GFP. A few mice (n=3) were co-injected with CAV2-GFP-CRE and CTb-647 for presence of HA in VSCTs labelled with CTb-647.

Mice were allowed to move freely in the open field assay with the Mouse NeuroBehavior Core at Columbia University. At P35-45, each mouse was injected intraperitoneally with 5mg/kg CNO (Tocris Cat. #4936). We opted to utilize the 5mg/kg CNO dose as it has been reported to be the optimal dosage for *in vivo* CNO injections (Manvich et al., 2018). Mice were then placed in the center of a clear Plexiglas arena (40 x 40 x 40 cm, Med Associates ENV-510) lit with dim light (~30 lux). Infrared beams embedded along the X, Y, Z axes of the arena automatically tracked distance moved and horizontal movement. Mice were allowed to ambulate freely for ~30 minutes. Data were collected into 10-minute intervals and total distance traveled for the first 10min after CNO injection and the last 10min for every hour (for the total of 6 hours) after CNO injection was analyzed using SOF-812 Activity Monitor software (Med Associates Inc.). The investigator was blind to the *in vivo* open field assay data set test which was revealed at the end of the analysis.

After the experiment was concluded, mice were euthanized and examined for quality of the injection by cerebellum fluorescence from the CTb under an epifluorescent microscope and from immunohistochemistry and confocal scanning of the L1 segment of the spinal cord.

Videography and analysis of swim test in adult mice

The temperature of the water bath was maintained at ~30C to avoid introducing temperature-bias measurements for all experiments. Mice were naïve in the swim test. Mice were tested once before CNO injection and 3 hours after 10mg/kg CNO injection. The swim test was set for 30sec to comply with IACUC guidelines. A high speed frame acquisition video camera was used for videography (Marshall, USB3.0) equipped with a 2.8mm IR1/2.5'' 3MP C lens. The camera was connected to a PC laptop using OBS Studio 27.0.1 (64bit) software. Videos were acquired at 60 frames per second (fps) at 1280x720 resolution. Videos were save in MKV format. For analysis, the software VLC 3.016 Vetinari was used. Videos were saved in MP4 format after analysis.

QUANTIFICATION AND STATISICAL ANALYSIS

Induction of locomotor-like activity and analysis

The L5 dorsal root or S3 dorsal root ganglion was placed into a suction electrode for stimulation to induce locomotor activity (10s, 4Hz, 0.2ms, 1.2-3x Threshold). Threshold was determined by the minimum intensity needed to evoke a response in 3 out of 5 consecutive trials at 0.1Hz. Locomotor-like activity was also induced following L5 ventral root stimulation (0.2 ms, 40-100μA, 0.1-10Hz) as well as through bath application of the pharmacological cocktail of drugs consisting of NMDA (5μM; Tocris), serotonin (10μM; Tocris), and dopamine (50μM; Tocris). Locomotor-like activity was defined by the three major criteria: i) cyclic rhythmic activity, ii) left-right alternation, and iii) flexor-extensor alternation (alternation between ipsilateral L1 and L5 spinal segments).

Quantification of the rhythmic activity in VSCT neurons was done using circular plots and circular statistics (Oriana v4.02). Locomotor cycle length was defined as the time between two consecutive flexor burst onsets (corresponding to 0 or 0°, for the first, and 1 or 360°, for the second, on a circular scale), for the spinal cord side ipsilateral to the recorded VSCT. Flexor bursts were defined as

bursting in the L1 or L2 segment motor neurons, whereas extensor bursts were defined as bursting in the L5 segment motor neurons. Onset of the flexor burst was defined as 50% of the time interval between trough and peak of the filtered (integrated by first low pass filtering at 200 Hz, followed by high pass filtering at 10 Hz, rectification and then low pass filtering at 3Hz) L1 or L2 segment motor neuron activity, as previously reported (Falgairolle et al., 2017).

The first VSCT action potential elicited during each burst of firing with respect to the recording from the homosegmental ventral root was analyzed. The timing of the onset of firing of the VSCT neuron compared to the onset of the flexor burst, normalized to the length of the locomotor cycle, was calculated. For each VSCT, the timing of the onset of action potential firing was plotted in a circular plot corresponding to the locomotor cycle. The mean timing of the first action potential was then calculated and plotted as a vector in the circular plot for each VSCT neuron. The length of the mean vector reflects how concentrated the values are around the mean vector, or the rhythmicity of that VSCT. To determine if the combined population of VSCTs exhibited rhythmic activity, the mean vector value from each of the individual VSCTs was then plotted in a circular plot corresponding to the locomotor cycle (Figure 3B_2). Using the Rayleigh Test, the statistical significance of the clustering of values around the mean vector was computed, reflecting whether that individual VSCT neuron fired in a rhythmic fashion. All recorded VSCT neurons had statistically significant rhythmic firing and were therefore included in further grouped analysis. The mean vector value, length of the mean vector, Raleigh Test Z Score, and p value for each of the 6 VSCT neurons were respectively: 1) 252 +/- 9°, 0.94, 3.5, $p < 0.05$; 2) 21 +/- 15°, 0.96, 2.8, $p < 0.05$; 3) 12 +/- 14°, 0.98, 2.9, $p < 0.05$; 4) 315 +/- 8°, 0.84, 3.6, $p < 0.05$; 5) 14 +/- 13°, 0.92, 3.4, $p < 0.05$; 6) 297 +/- 2°, 0.98, 4.75, $p < 0.01$. To determine if the combined population of VSCT neurons exhibited rhythmic activity, the mean vector value from each of the individual VSCT neurons was then plotted in a circular plot corresponding to the locomotor cycle. The mean timing of the first action potential for the population was calculated and plotted as a vector in a circular plot and the Rayleigh Test was conducted to test for statistical significance.

Statistics

The locomotor-like activity analysis of rhythmic activity in VSCT neurons used circular statistics. For this analysis, statistical analysis was performed using Oriana v4.02. Statistical analysis was carried out with the Rayleigh Test. P values are indicated as follows: * = $P < 0.05$; ** = $P < 0.01$; *** = $P < 0.001$, with $P < 0.05$ considered statistically significant. For all other analysis, statistical analysis was performed using GraphPad Prism 6. All results are expressed as means ± standard error of the mean (SEM). Statistical analysis was carried out with the two-tailed unpaired Student's t-test, the two-tailed paired Student's t-test, or with one-way ANOVA, as appropriate. *Post-hoc* analysis of one-way ANOVA statistical tests was conducted with Tukey's *post hoc* test. P values are indicated as follows: * = $p < 0.05$; ** = $p < 0.01$; *** = $p < 0.001$, with $p < 0.05$ considered statistically significant. No randomization was used.

CellPress
OPEN ACCESS

Supplemental figures

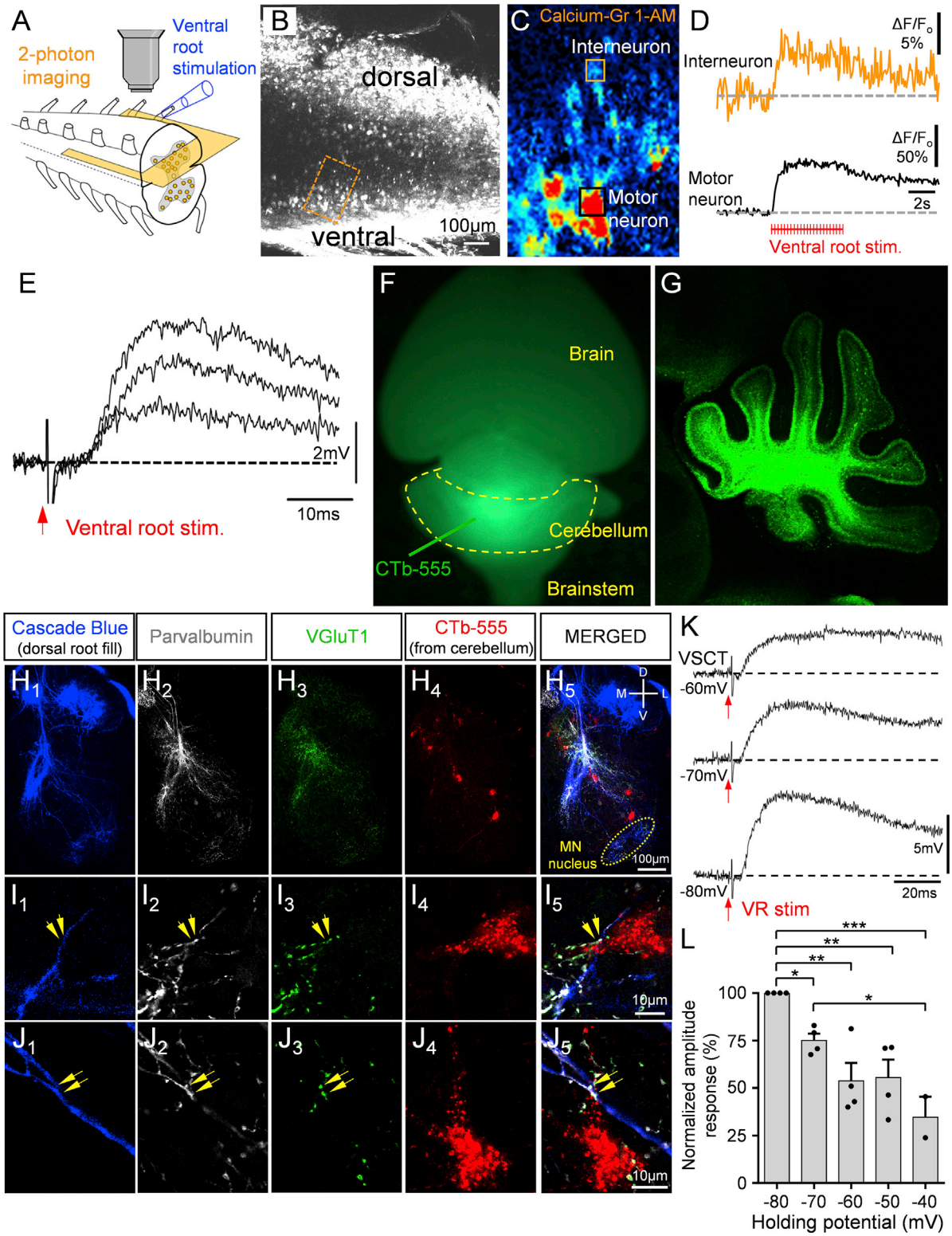

(legend on next page)

Figure S1. A set of interneurons located dorsolateral and close to the motor neuron nucleus is activated following motor neuron axon stimulation; injection of CTb in cerebellum to label SCT neurons; VSCT neurons receive proprioceptive synapses and EPSP responses in a VSCT neuron after ventral root stimulation, related to Figures 1 and 2

(A) Schematic illustrating the experimental approach in which the dye calcium green 1, indiscriminately labeled spinal cord neurons by electroporation. 2-photon laser imaging of fluorescence representing calcium entry into the neuron was performed through the lateral side of the spinal cord at P3–P5 following ventral root electrical stimulation.

(B) Low-magnification view of fluorescent signal of the spinal cord from the lateral side. The ventral and dorsal side of the spinal cord is denoted. Orange dotted box is shown enlarged in (C).

(C) Change in calcium signal over its baseline fluorescence following ventral root stimulation. Two regions of interest (ROIs) are shown for a motor neuron (black box) and a dorsal interneuron (orange box). These neurons were not Renshaw cells since they are located ventrally to the motor neuron nucleus. In addition, they are not likely to be $Sim1^+$ interneurons since this neuronal type is deep within the intermediate gray matter.

(D) $\Delta F/F_o$ calcium signal for the ROI over the spinal interneuron (orange box in C), and a motor neuron (black ROI in C). Following ventral root stimulation, motor neurons exhibited a large increase in fluorescence change, whereas interneurons exhibited smaller calcium signals (N = 4 mice).

(E) Intracellular whole-cell patch clamp traces from an interneuron (targeted visually) revealing graded and short latency excitatory post-synaptic potentials following homosegmental ventral root stimulation.

(F) Fluorescence image from a P4 mouse that was injected with CTb-555 in the cerebellum at birth (P0).

(G) Confocal image from a P4 cerebellum section showing the specificity of the injected CTb-555 within cerebellum injected at P0.

(H) (H_{1-5}) Confocal images with dorsal root orthogradely filled sensory fibers with Cascade Blue Dextran (in blue, H_1), Parvalbumin (in white, H_2), VGluT1 (in green, H_3) immunoreactivity and CTb-555 labeled SCT neurons (in red, H_4). Merged image is shown in H_5. The approximate location of the motor neuron nucleus is denoted by yellow dotted oval shape in H_5.

(I and J) Higher magnification images are shown for a VSCT neuron receiving proprioceptive synapses on the soma (I_{1-5}) and on a proximal dendrite (J_{1-5}). Yellow arrows denote synapses that co-localize Cascade Blue, VGluT1 and Parvalbumin in apposition to a VSCT neuron. D: dorsal; V: ventral; L: lateral; M: medial.

(K) EPSPs from a P3 L1 VSCT neuron at different holding potentials following L1 ventral root stimulation. Red arrows indicate the stimulus artifact.

(L) Normalized EPSP amplitude (with respect to the response at −80 mV) at different holding potentials in VSCT neurons (n = 4 VSCT, N = 4 mice) following ventral root stimulation. (−80 versus −70: *$p < 0.05$; −80 versus −60: **$p < 0.01$; −80 versus −50: **$p < 0.01$; −80 versus −40: ***$p < 0.001$; −70 versus −40: *$p < 0.05$; one-way ANOVA, Tukey's post hoc test.)

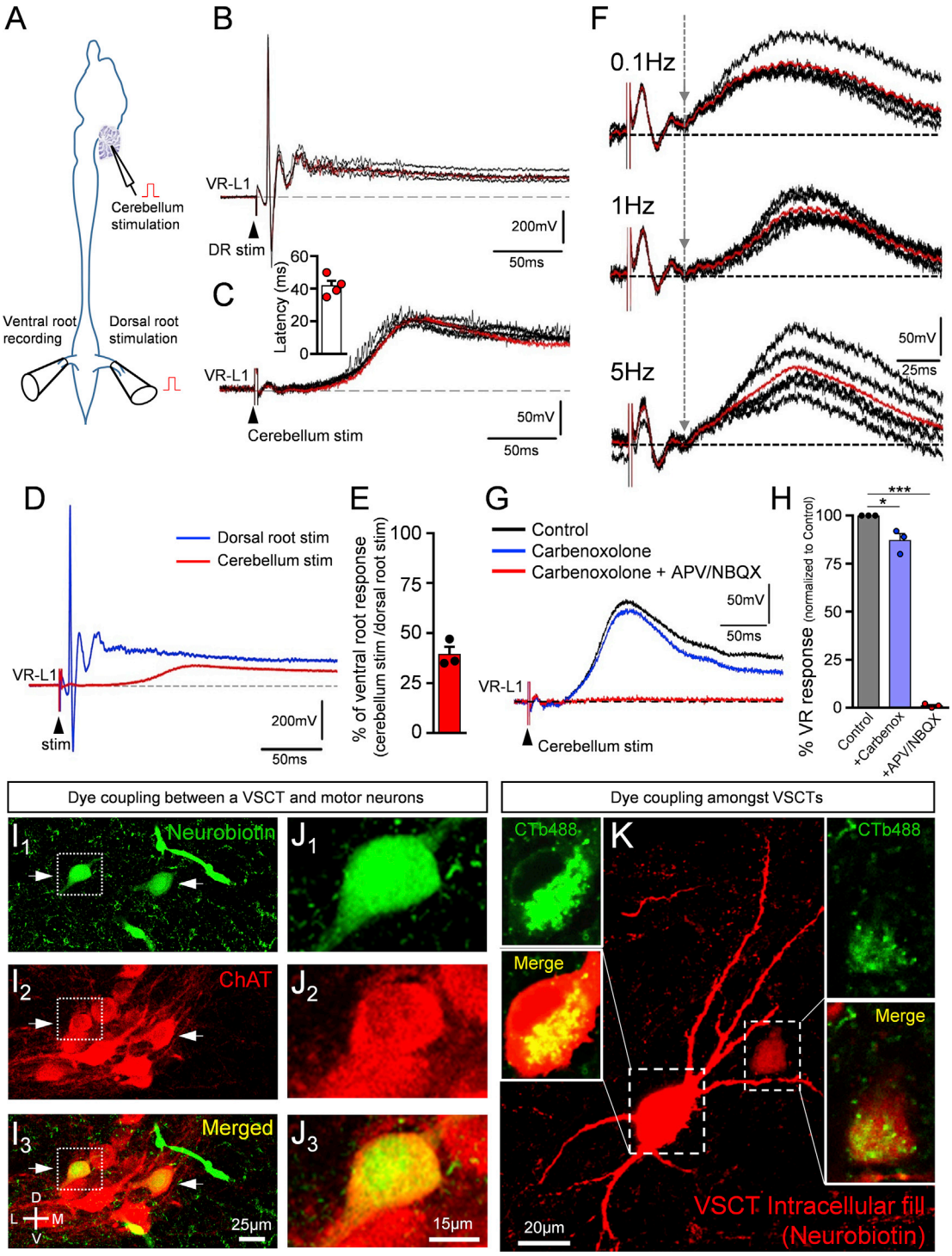

Figure S2. Minimal spread of current from VSCTs to motor neurons and dye coupling between VSCTs and motor neurons and among VSCT neurons, related to Figure 2

(A) Schematic of experimental setup. A stimulating electrode was place in the cerebellum (vermis) and in the L1 dorsal root, while motor neuron responses were recorded from the L1 ventral root.

(B) Five superimposed ventral root (L1) responses recorded following L1 dorsal root stimulation at 0.1 Hz. Red trace is the average response.

(C) Five superimposed ventral root (L1) responses following cerebellum stimulation at 0.1 Hz. Red trace is the average response. Inset shows the latency of the onset of response in four different experiments (N = 4 mice).

(D) Two superimposed VR-L1 average responses following dorsal root (blue) and cerebellum stimulation (red).

(legend continued on next page)

(E) The area of the ventral root response following cerebellum stimulation is expressed as a percentage of the ventral root response following dorsal root stimulation. The area of the response was measured for the first 250 ms after the stimulus (N = 3 mice at P4 and P5).
(F) Superimposed ventral root responses at three different frequencies (0.1, 1, and 5 Hz) of cerebellum stimulation. Red trace is the average response. Dotted vertical line with arrows indicate the same latency of the onset of response, indicative of monosynapticity.
(G) Superimposed average responses in control solution (black), 30 min after 100 μM carbenoxolone (blue) and 15 min after addition of 100 μM APV and 20 μM NBQX (red).
(H) Percentage expression of ventral root responses under carbenoxolone (blue) and addition of APV/NBQX (red), normalized to control solution (gray) (N = 3 mice). *$p < 0.01$, ***$p < 0.001$, ANOVA, post hoc: Tukey's multiple comparisons test.
(I) ($I_{1–3}$) Single optical plane confocal images showing neurobiotin (revealed post hoc with the avidin-biotin complex; green) intracellularly filled in a P4 L2 VSCT neuron and diffused into motor neurons (revealed with ChAT immunoreactivity; shown in red). Two motor neurons (white arrows) show co-localization of neurobiotin and ChAT (yellow). Note that the recorded VSCT is not shown, since it was located in a different spinal cord section (n = 4 VSCTs from N = 4 mice).
(J) ($J_{1–3}$) Enlarged confocal images from the dotted boxes in (I) showing co-localization of neurobiotin (green) and ChAT (red).
(K) Confocal image from a z stack showing the intracellular recorded and filled P4 L2 VSCT neuron with neurobiotin (red) next to a weakly filled red-labeled VSCT neuron (also labeled with CTb-488). Insets show the two VSCT neurons at higher magnification co-localizing with CTb-488 (n = 4 VSCTs from N = 4 mice).

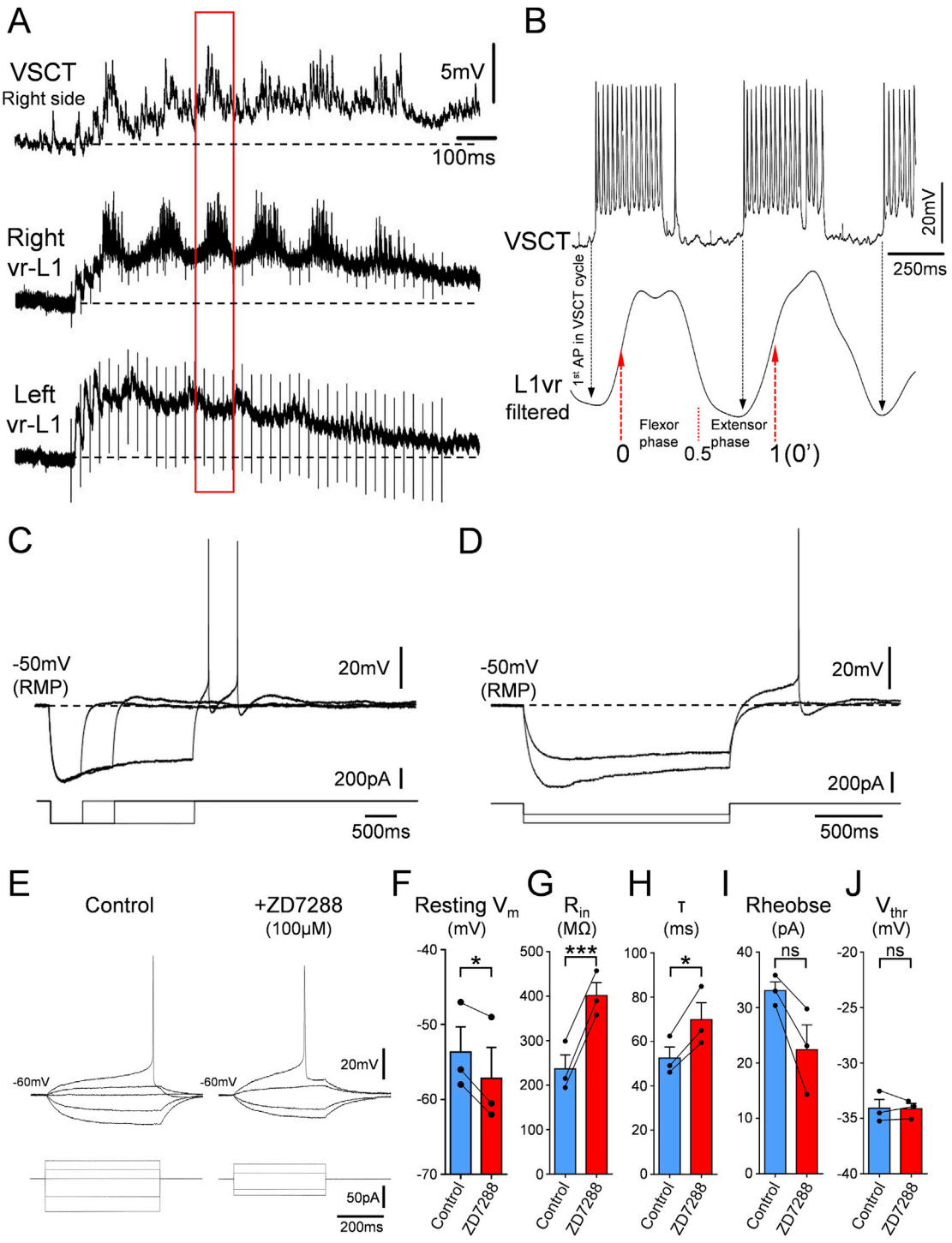

Figure S3. Subthreshold rhythmic oscillations in VSCT neurons, analysis of the rhythmic firing of VSCTs during locomotor-like activity and time- and voltage- dependency of sag, and post-inhibitory rebound in VSCTs, related to Figure 3

(A) Intracellular recording from an L1 VSCT neuron (top trace) and extracellular recordings from the right (middle trace) and left (bottom trace) L1 ventral roots, during locomotor-like activity induced by dorsal root stimulation. The resting potential of the VSCT neuron was −65 mV. Red box indicates that the VSCT neuron was in phase with the homosegmental ventral root.

(B) An intracellular response from a P4 L1 VSCT neuron exhibiting rhythmic bursts of action potentials along with a filtered extracellular trace from the ipsilateral homosegmental L1 ventral root during locomotor-like activity induced by electrical stimulation of an adjacent (L2) ventral root. Time point 0 (1) was the beginning of the locomotor cycle, defined as the point at which the trace reaches 50% of the amplitude between trough and peak in the flexor phase. The timing of the first

(legend continued on next page)

action potential (AP) of the VSCT neuron during each burst was determined in comparison to the locomotor cycle. Note that the VSCT neuron fires APs before the onset of motor neuron activity. See STAR Methods for further details.
(C) Superimposed traces from a P4 L2 VSCT neuron exhibiting a time-dependent sag and post-inhibitory rebound to negative current injection.
(D) Superimposed traces from a P4 L2 VSCT neuron illustrate that the sag and post-inhibitory rebound are also voltage-dependent.
(E) Current-voltage superimposed responses before and during ZD7288 exposure in a VSCT neuron.
(F–J) Exposure to ZD7288 (data in red) decreased the resting membrane potential (F), increased the input resistance (G), increased the time constant (H), reduced the rheobase (I), and did not alter the voltage threshold (J) in VSCT neurons (n = 3 VSCTs from N = 3 mice). Ns: not significant ($p > 0.05$), *$p < 0.05$, ***$p < 0.001$, two-tailed paired t test.

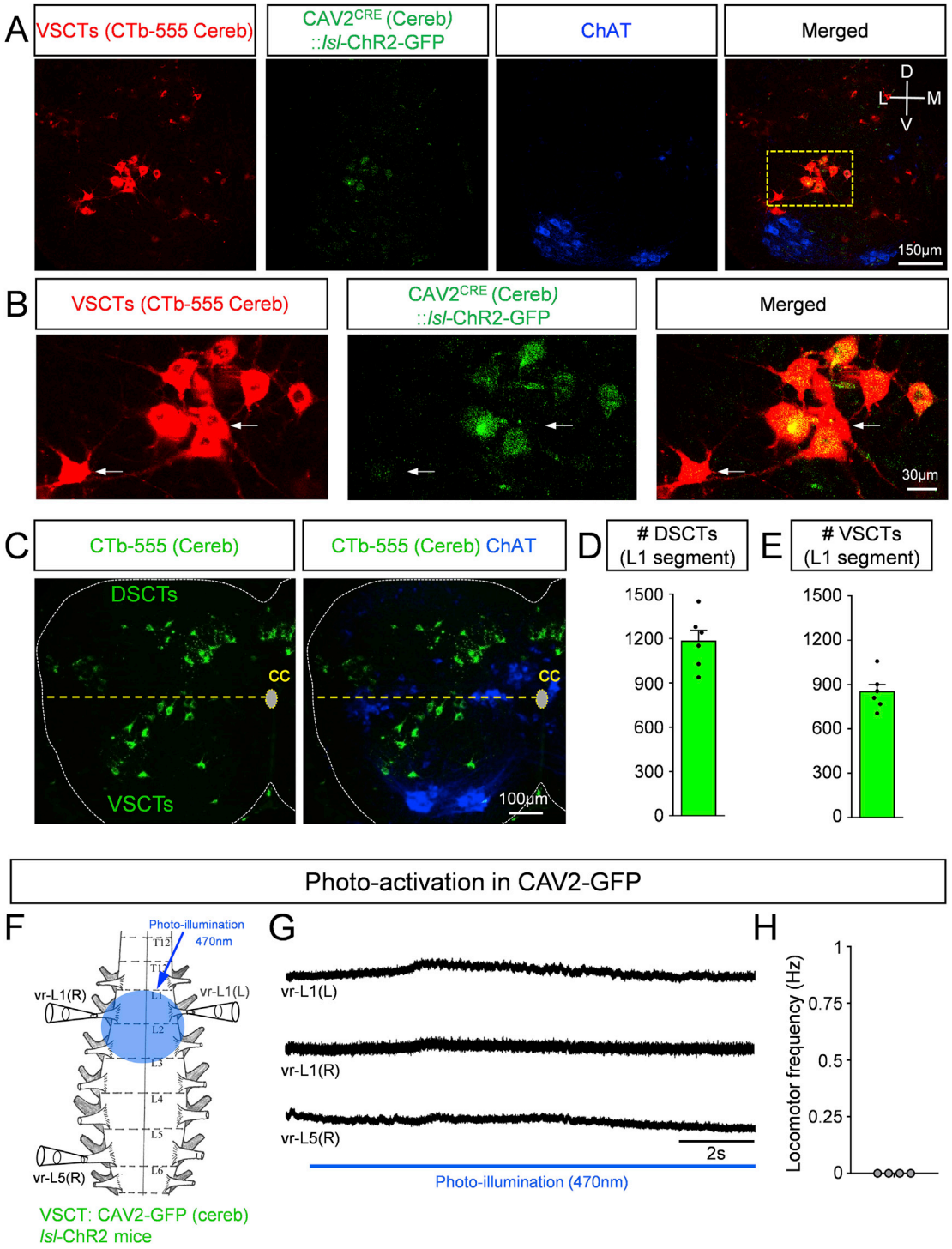

Figure S4. GFP expression in VSCTs, quantification of DSCTs and VSCTs, and CAV2 or retinal do not produce locomotor-like behavior following photo-illumination, related to Figure 4

(A) Low-magnification confocal images from the ventral horn of a mouse in which CAV2-Cre was introduced into VSCTs to express ChR2 in *lsl*-ChR2-GFP mice. CTb-555 (in red) was co-injected into the cerebellum at P0 to retrogradely label VSCT neurons. GFP (in green) was only observed in VSCT neurons labeled with CTb-555. Motor neurons are labeled with ChAT immunoreactivity (in blue). Merged image of all signals is shown on the right side. Dotted rectangular denotes the area shown at higher magnification in (B).

(legend continued on next page)

(B) Higher magnification images from (A) showing VSCT neurons co-localizing CTb-555 (red) and GFP (green). White arrows indicate two VSCT neurons not labeled with GFP (N = 4 mice). The GFP signal is weak since the spinal cord was immersion fixed in 4% paraformaldehyde after the completion of the physiological experiment. Every spinal cord was examined after each physiological experiment.
(C) Confocal images showing CTb-555^{+} neurons. All neurons dorsal to the medio-lateral line (yellow dotted line) starting at the central canal (cc) were considered as dorsal spinocerebellar tract (DSCT) neurons, while neurons ventral to the dotted line were considered as ventral spinocerebellar tract (VSCT) neurons. ChAT immunoreactivity is shown in blue.
(D) The total number of DSCT neurons in the L1 spinal segment. Each point is the total number of DSCTs in a single mouse (N = 6 mice).
(E) The total number of VSCT neurons. Each point is the total number of VSCTs in the L1 segment from a single mouse (N = 6 mice). For the counting details see STAR Methods.
(F) Schematic illustration of the L1 and L2 segments photo-illuminated from the ventral aspect with a 470 nm LED in control preparations in which the cerebellum was injected with CAV2-GFP at P0 in *lsl*-ChR2 mice.
(G) Retinal was applied in the bath at 1–3 μM and photo-illumination revealed no effects in the corresponding ventral roots.
(H) Quantification of the responses after photo-illumination in spinal cords in which VSCT neurons were transduced with CAV2-GFP (N = 4 mice).

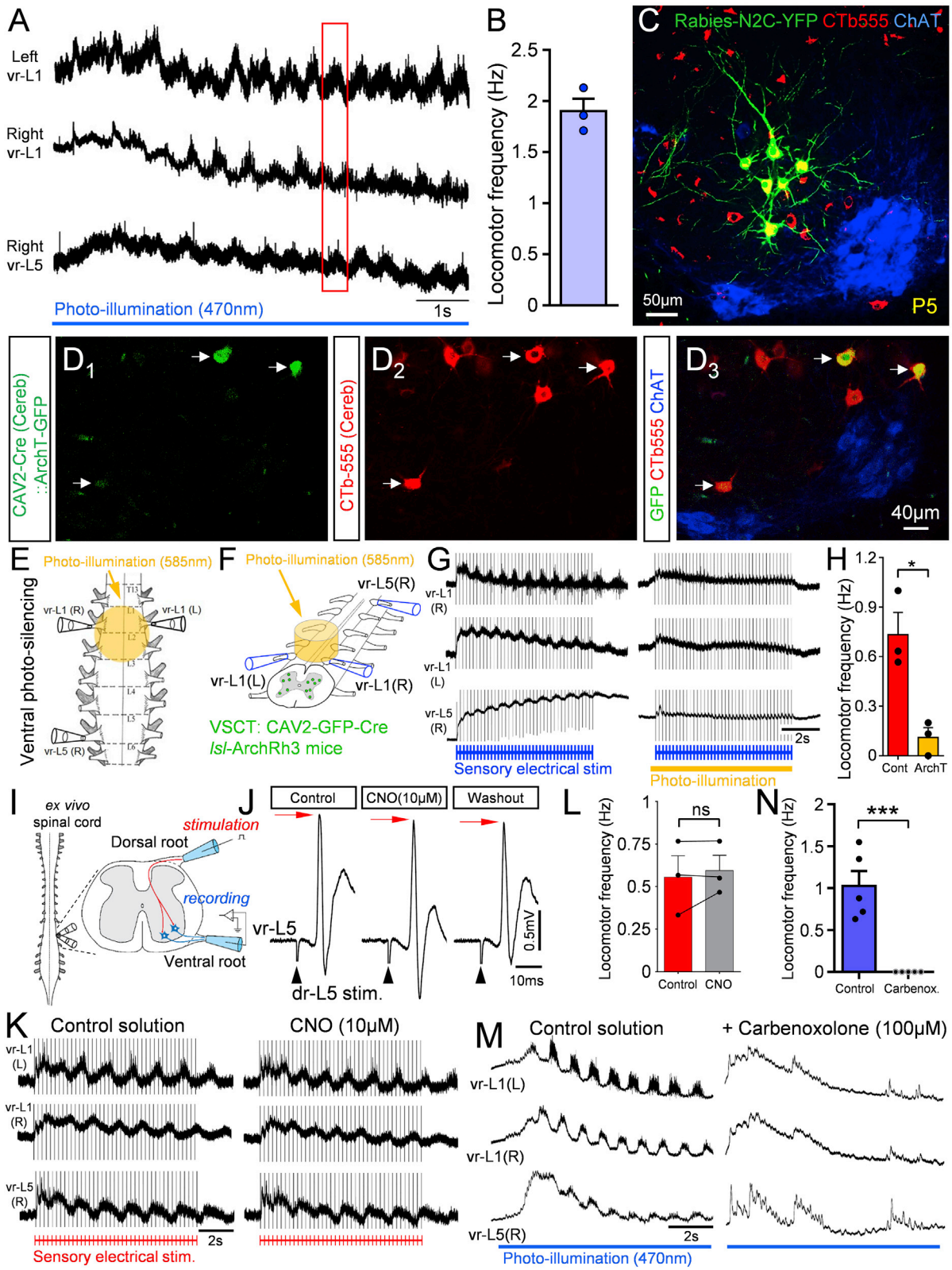

(legend on next page)

Figure S5. Photo-activation of VSCTs expressing ChR2-GFP introduced by the N2C-Rabies induces locomotor activity; optogenetic silencing of VSCTs via Archaerhodopsin-3 degrades locomotor activity; CNO does not alter synaptic transmission or motor neuron function; CAV2-GFP in VSCTs or exposure to CNO does not have any significant effects in locomotor activity; abolition of locomotor activity induced by photoactivation of VSCTs in L1/L2 after carbenoxolone; related to Figures 4 and 5

(A) Rhythmic activity in a P5 mouse *ex vivo* preparation following photo-activation (in the L1/L2 segments) of VSCT neurons with a 470 nm LED (bottom blue trace). Extracellular traces from the left and right L1 ventral roots and the right VR-L5. Red box illustrates the alternating activity among the different roots.

(B) Quantification of the locomotor frequency following photo-activation of VSCTs (N = 3 mice).

(C) Confocal image from a P5 mouse spinal cord, showing CTb-555^{+} spinocerebellar tract neurons (in red) and GFP (in green) following concomitant injection with the rabies-N2C expressing ChR2 and GFP. Motor neurons are labeled with ChAT (in blue).

(D) (D_{1-3}) Confocal images from a P4 mouse showing VSCT neurons expressing GFP (green, D_1) and CTb-555 (red, D_2); motor neurons were revealed by ChAT immunoreactivity (blue, merged in D_3). White arrows show three VSCT neurons which co-express GFP and CTb-555. CTb-555 was injected into the cerebellum at P0 to retrogradely label VSCT neurons along with CAV2 driving Cre expression in a *lsl*-Archaerhodopsin-3-GFP (ArchT) mouse to introduce Archaerhodopsin-3 to VSCT neurons (N = 3 mice).

(E and F) Schematics of the experimental protocol illustrating the bilateral illumination of the L1 and L2 segments with a 585 nm LED from the ventral aspect, while motor neuron activity was monitored through bilateral L1s and L5 segment ventral roots with extracellular electrodes.

(G) Extracellular responses from ventral roots exhibiting locomotor-like activity following sensory fiber electrical stimulation (blue line at the bottom; 4 Hz for 10 s) in control condition and following photo-illumination with 585 nm LED (right) in a P5 *ex vivo* spinal cord preparation. Yellow line represents the duration of photo-illumination.

(H) Quantification of the locomotor frequency before (red) and after (yellow) photo-silencing of VSCT neurons. *$p < 0.05$; two-tailed Student's t test (N = 3 mice).

(I) Schematic of the *ex vivo* spinal cord preparation and magnification of the transverse section of the spinal cord to denote the extracellular electrodes for stimulation of the dorsal root and recording from the ventral root.

(J) Extracellular monosynaptic response in L5 motoneurons following L5 dorsal root stimulation at P5 in *ex vivo* spinal cord preparation in which the inhibitory DREADDs receptor was introduced to VSCTs at P0 by cerebellum injections of CAV2-Cre in a *lsl*-hM4Di (inhibitory DREADDs) mouse. Note that application of CNO elicited no change in the monosynaptic response (N = 3 mice).

(K) Extracellular recordings from control experiments in which CAV2-GFP was injected into the cerebellum at P0 in *lsl*-hM4Di mice. At P4, under control artificial cerebrospinal fluid, electrical stimulation of sensory fibers elicited locomotor-like activity (left side). Bath application of 10 μM clozapine N-oxide (CNO) had no effect on the locomotor frequency induced by sensory fiber stimulation (right side).

(L) Quantification of the locomotor frequency before and after CNO application (N = 3) (two-tailed Student's t test).

(M) Locomotor-like activity evoked from a P4 spinal cord in which VSCT neurons express ChR2 where photo-activated with a 470 nm LED (denoted by the blue lines under the traces) under control solution and after 100 μM carbenoxolone. The area of photo-illumination was in the L1/L2 spinal segments from the ventral side. Locomotor activity was abolished after bath application of carbenoxolone.

(N) Quantification of the locomotor frequency following photoactivation of VSCTs before and after bath application of carbenoxolone. ***$p < 0.001$; two-tailed Student's t test (N = 5 mice).

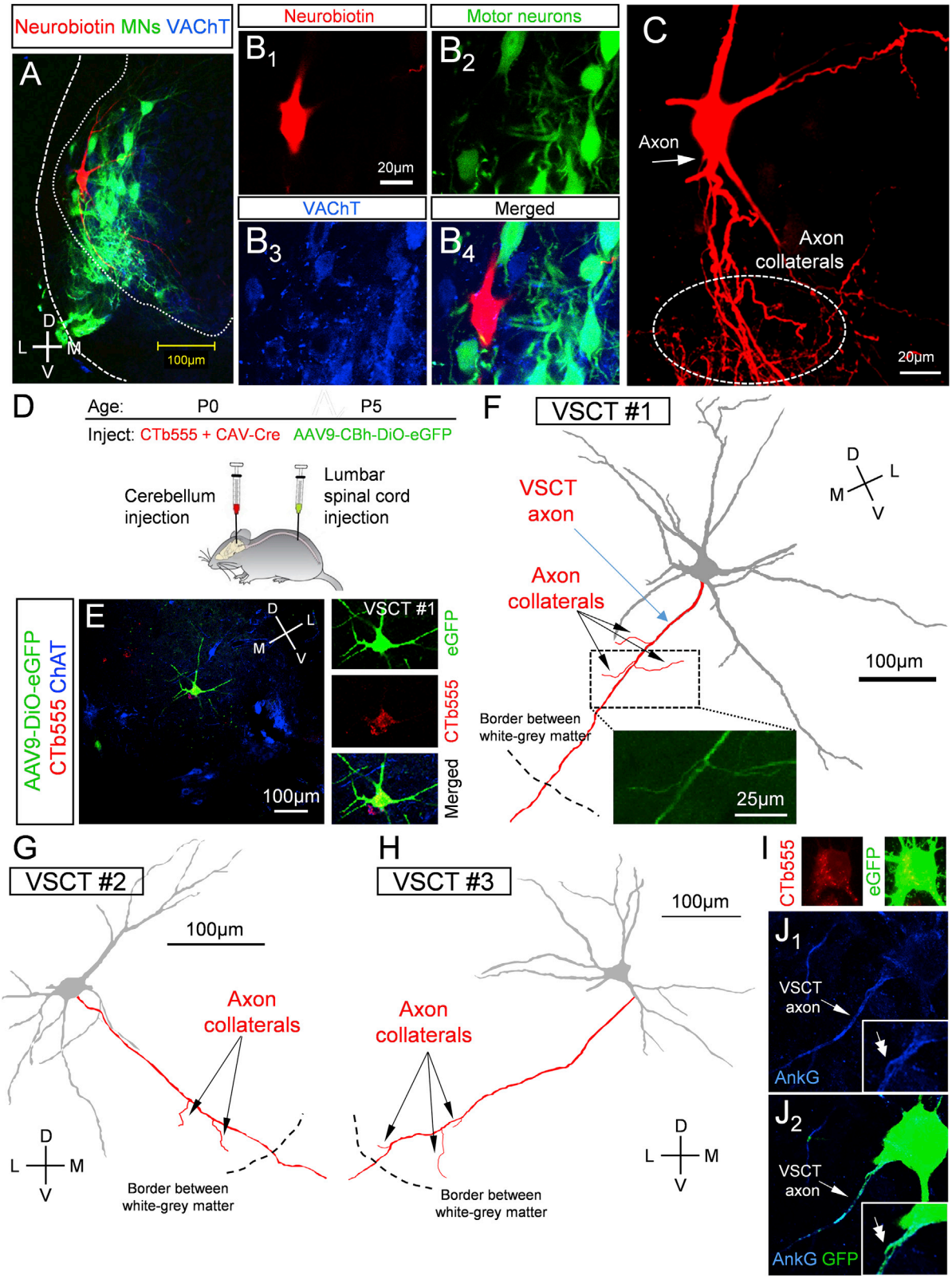

(legend on next page)

Figure S6. Visualization of VSCT axon collaterals, related to Figure 6

(A–C) A P3 L1 VSCT neuron filled with neurobiotin, revealed with the avidin-biotin complex (red, B_1). Motor neurons are in green (B_2, labeled with fluorescein dextran dye retrogradely applied to the L1 ventral root) and vesicular acetylcholine transporter (VAChT, B_3) immunoreactivity is in blue. Single optical confocal plane images of all fluorochromes in (B_1–B_4). Note the abundant arborization of ipsilateral axon collaterals in (C) from a z stack projection (total z axis: 75 μm).

(D) CTb-555 and CAV-Cre was injected in the cerebellum at birth (P0), while AAV9-CBh-DiO-eGFP was injected in the lumbar spinal cord at P5. Spinal cords were examined at P12.

(E) Confocal image showing a VSCT neuron transfected with AAV9-CBh-DiO-eGFP (in green), CTb-555 (in red) and ChAT immunoreactivity (in blue). Insets show at higher magnification the co-localization of CTb-555 and GFP.

(F) The VSCT neuron shown in (B) was reconstructed with Neurolucida (VSCT#1). The somato-dendritic morphology is shown in gray, while the axon and its collaterals are shown in red. Dotted box shows the confocal image of the main axon and two of its axon collaterals.

(G and H) Two additional VSCT neurons (VSCT#2 and #3) reconstructed with Neurolucida showing their main axon and their collaterals (arrows) (n = 7 VSCTs from N = 3 mice). Dotted lines denote the gray-white matter border.

(I) Co-localization of GFP and CTb-555 in another VSCT neuron.

(J) ($J_{1,2}$) The main axon of the VSCT shown in (I) was identified by ankyrin G (AnkG) immunoreactivity (in blue; arrow). Insets show that an axon collateral also expressed AnkG (double arrowhead).

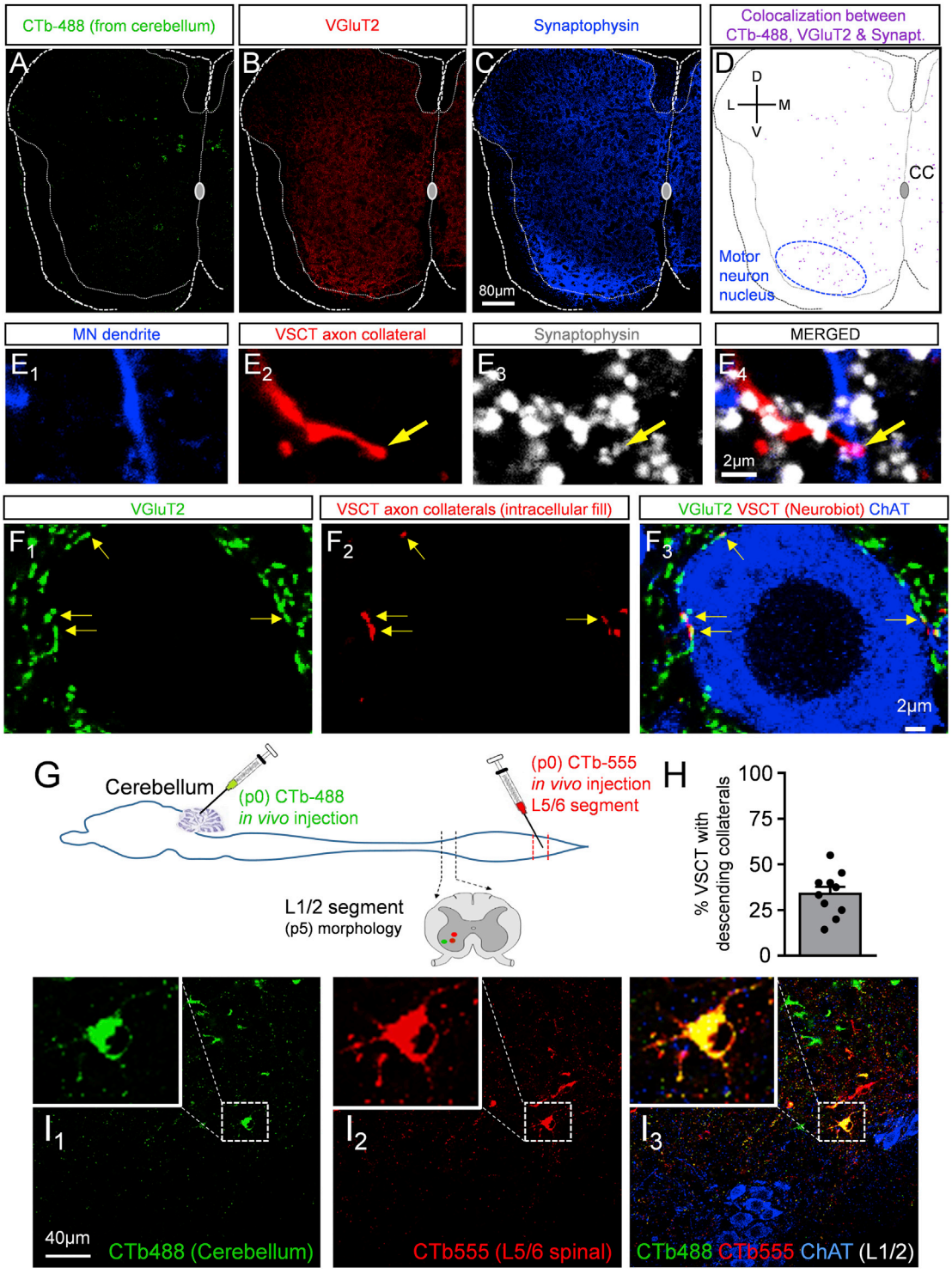

Figure S7. Arborization of synapses from spinocerebellar tract neurons in the L1/L2 spinal cord; VSCT axon collaterals contact motor neurons and VSCT neurons possess descending axon collateral projections to caudal lumbar segments, related to Figure 6

(A–C) Single optical plane confocal images in the L1 spinal cord from CTb-488 (A, in green) injected in the cerebellum at birth, immunoreactivity against VGluT2 (B, in red) and synaptophysin (C, in blue).

(D) Points in purple indicate the location of synapses that co-localized CTb-488, VGluT2, and synaptophysin. Co-localization was determined through image processing using ImageJ. Note that the co-localization points are not to scale and have been enlarged to improve visibility. Similar results were observed in N = 4 mice.

(legend continued on next page)

(E) (E_{1-3}) Single optical plane confocal images showing a VSCT axon collateral from a P4 L2 VSCT neuron filled with neurobiotin and revealed with the avidin-biotin complex (red, E_1), a motor neuron (MN) dendrite (blue, E_2) labeled with Cascade Blue Dextran dye applied retrogradely from the cut ventral root and synaptophysin immunoreactivity (white, E_3). (E_4) Merged image showing a putative site of contact (yellow arrow) between a VSCT axon collateral and a motor neuron dendrite (n = 5 VSCTs from N = 5 mice).

(F) (F_{1-3}) Single optical plane confocal images showing VGluT2 immunoreactivity (F_1), axon collateral(s) from a P4 VSCT neuron, filled with neurobiotin (F_2; red) and ChAT immunoreactivity (F_3; blue). Four putative sites (yellow arrows) of synaptic contacts were observed on the motor neuron soma (n = 3 VSCTs from N = 3 mice).

(G) CTb-488 was injected into the cerebellum to label VSCT neurons (green) at P0. Concomitantly, CTb-555 was also injected *in vivo* into the L5/L6 spinal cord (red). At P5, the L1 and L2 spinal segments were sectioned and examined for co-localization of the two tracers.

(H) Percentage of VSCT neurons co-expressing CTb-555 and CTb-488 (as shown in I_3), compared to VSCT neurons expressing CTb-488 only. Individual data points denote numbers of VSCTs from 75 μm thick transverse sections from three experiments (N = 3 mice).

(I) (I_{1-4}) Single optical plane confocal images from the L1/L2 segments containing a VSCT neuron with both fluorochromes co-localized (yellow in I_3), demonstrating the presence of descending axon collaterals from L1/L2 segment VSCT neurons. The motor neuron location was revealed by ChAT immunoreactivity (I_3, blue).

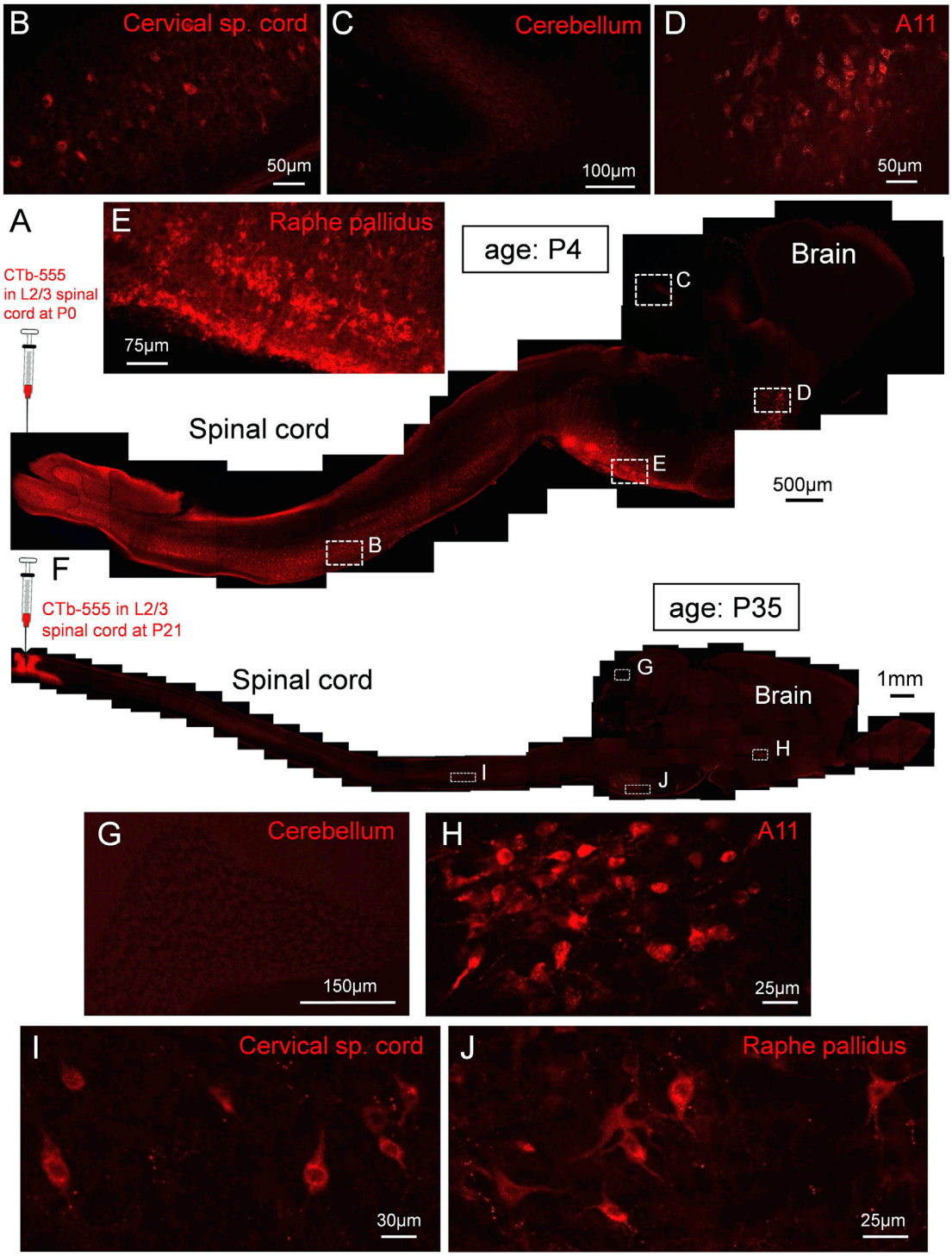

Figure S8. No direct connections from the cerebellum to the lumbar spinal cord during early mouse development and in adult mice, related to Figure 7

(A) CTb-555 was injected *in vivo* in the L2/L3 lumbar spinal cord at birth (P0). At P4 (N = 6 mice), the entire spinal cord and brain was dissected, sectioned and imaged with a confocal microscope. Montage of confocal images is shown.

(B–E) Higher magnification images (shown in dotted boxes) of: the cervical spinal cord (B) which contains propriospinal interneurons, cerebellum (C), indicating the absence of neurons with CTb-555, unlike the A11 region (D), which contains dopaminergic neurons, as well as and the Raphe pallidus (E), which contains serotonergic neurons. These neurons are all known to send axons in the lumbar spinal cord.

(legend continued on next page)

(F) CTb-555 was injected *in vivo* in the L2/L3 lumbar spinal cord at P21. At P35 (N = 4 mice), the entire spinal cord and brain was dissected, sectioned and imaged with a confocal microscope. Montage of confocal images is shown the entire mouse CNS.
(G–J) Higher magnification images shown in dotted boxes in (A) of: cerebellum (G), indicating the absence of neurons with CTb-555, unlike the dopaminergic neurons of A11 region (H), as well as the propriospinal interneurons in the cervical spinal cord (I) and the serotonergic neurons in the Raphe pallidus (J), which are all known to send axons in the lumbar spinal cord.

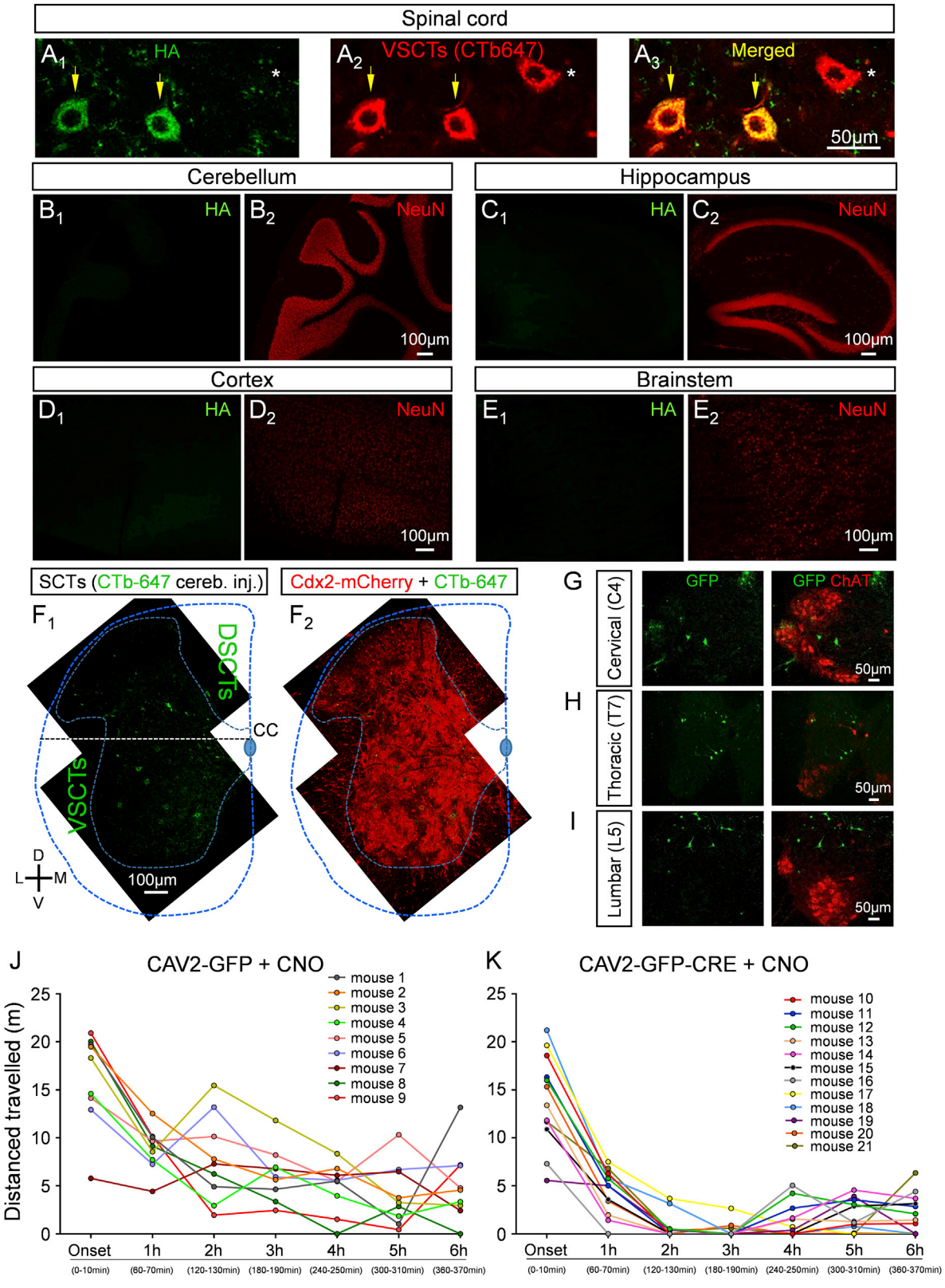

(legend on next page)

Figure S9. The inhibitory DREADDs receptor is selectively expressed in VSCT neurons in vivo; VSCT neurons are expressed throughout the spinal cord; distance travelled in Cdx2^{FlpO}::*fsf-lsl*-h4MDi mice after CNO following cerebellar injection with CAV2-GFP or CAV2-GFP-CRE, related to Figure 7

(A) (A_{1-3}) *fsf-lsl*-hM4Di mice were crossed with Cdx2^{FlpO} mice and the resulting pups were injected into the cerebellum at P21 with a combination of CTb-555 (to label VSCTs) and CAV2-GFP-Cre (to introduce the inhibitory DREADDs receptor specifically to VSCTs). Immunohistochemistry at P45 against hemagglutinin (HA), co-expressed (yellow arrows) with the inhibitory DREADDs receptor, reveals specific co-localization with CTb-555. Asterisk shows a CTb-555^{+} VSCT neuron that did not express HA (N = 3).

(B–E) Absence of HA immunoreactivity in cerebellum (B), hippocampus (C), cortex (D) and brainstem (E). NeuN immunoreactivity is shown in red.

(F) (F_{1-3}) Cdx2-mCherry signal amplified with DsRed immunoreactivity in a P45 L2 spinal cord injected with CTb-647 (F_2) at birth to label spinocerebellar tract neurons (F_3 is a merged image) (N = 7 mice). VSCT neurons were distinguished from DSCT neurons, as the neurons located ventrally to the white dotted line from the central canal (cc) to the lateral edge of the white-gray matter (annotated by light blue dotted line) as shown in F_2. D: Dorsal, V: ventral, L: lateral, M: medial.

(G–I) Confocal images of GFP immunoreactivity (green), ChAT immunoreactivity (red) in the C4 cervical segment (G), T7 thoracic segment (H) and L5 lumbar segment (I) from a Cdx2^{FlpO}::*fsf-lsl*-h4MDi mouse (n = 7 mice) that was injected in the cerebellum with CAV2-GFP-Cre.

(J and K) The distance traveled for 10 min at the onset and every hour after 5 mg/kg CNO (i.p.) injection in Cdx2^{FlpO}::*fsf-lsl*-h4MDi mice (age: P35–P45) which received cerebellar injections at P21 with either CAV2-GFP (J) as a control (N = 9 mice), or CAV2-GFP-Cre (N = 12 mice) (K). Each mouse is color-coded in each of the two experimental groups.